IMPROVEMENTS TO A HIGH-ATTITUDE WIND-TUNNEL STING SYSTEM FOR IMPROVED DATA QUALITY

A Thesis

by

MATTHEW QUINN MILLER

Submitted to the Office of Graduate and Professional Studies of
Texas A&M University
in partial fulfillment of the requirements for the degree of

MASTER OF SCIENCE

Chair of Committee,	Edward White
Committee Members,	John Valasek
	Kiju Lee
Head of Department,	Srinivas Rao Vadali

May 2021

Major Subject: Aerospace Engineering

Copyright 2021 Matthew Quinn Miller

ABSTRACT

Successful wind tunnel testing requires careful attention to how model mounts may affect data quality. In several past sting-mounted tests at the Oran W. Nicks Low-Speed Wind Tunnel (LSWT), the High-Attitude Robotic Sting (HARS) pitch/roll actuator system has been suspected to cause undesirable aerodynamic interference in collected data. The size of the mounting bracket and roll actuator "bullet" fairing causes undesirable upflow at the aft end of sting-mounted models. Furthermore, the motors that drive position of the HARS assembly introduce excessive electronic noise. This makes data collection from sensitive instrumentation like accelerometers nearly impossible.

This thesis details the design changes to the HARS system that mitigate these sources of aerodynamic and electronic interference. The HARS bullet was completely redesigned and rebuilt to decrease its diameter from 10.5 inches to 6.0 inches. Additionally, all drive components and motors were replaced by new motors with passive holding brakes to improve functionality and decrease electronic noise.

Performance was verified using a 6.25%-scale WB-57 aircraft tested at the LSWT in 2014. Differences in aerodynamic performance data measured by an internal balance were compared and analyzed for differences between the redesigned system and the previous system. Additionally, accelerometer data was compared for differences in noise reduction by the new motors. The redesigned system and components show clear improvements to data quality, both in aerodynamic force and moment coefficients as well as accelerometer data. These improvements will allow more accurate measurements and allow more sensitive measurement techniques to be utilized, expanding the HARS system capabilities.

ACKNOWLEDGMENTS

I would first like to thank my committee chair and graduate advisor, Dr. White, for your guidance and support over these past four years I've known you. I've been incredibly lucky to have had the chance to work at the LSWT as an undergraduate, and continuing to work there during graduate school I feel has opened up so many opportunities for me to learn and experience the engineering industry.

I would also like to thank my committee member, Dr. Valasek, without whom I never would have had the chance to work at the LSWT in the first place. We first met when you were the interim Engineering Honors advisor in fall of 2016, when you introduced me to Dr. White and recommended that I applied to work for the LSWT. This has started me on a hopefully long path of future test engineering, and I am grateful that we have had the opportunity to meet.

Lastly, I would like to thank the LSWT staff and student workers, past and present. I've learned so much over the past four years, and I am incredibly fortunate to have had such a fun, supporting, and understanding group of people to work with.

TABLE OF CONTENTS

Page

LIST OF FIGURES

FIGURE Page

LIST OF TABLES

TABLE Page

1. INTRODUCTION

1.1 Motivations for Research

The Oran W. Nicks Low-Speed Wind Tunnel (LSWT) at Texas A&M University (TAMU) is a closed-loop wind tunnel with a 7 ft $\times$ 10 ft test section capable of speeds up to 200 mph (approximately Mach 0.25), or a dynamic pressure of $q = 100$ psf. Higher velocities up to Mach 0.4 can be achieved with a 7 ft $\times$ 7 ft reduced area test section. Since the late 1950s, the LSWT has been extensively used for commercial testing, academic research, and undergraduate teaching.

At the LSWT, aerodynamic forces and moments are typically measured using the six-component pyramidal external balance under the test section floor or using a sting-mounted internal balance supported by the pitch/roll actuator. That actuator is referred to as the High-Attitude Robotic Sting (HARS). The removable HARS system provides pitch and roll control of sting-mounted models while maintaining model position in the center of the test section; yaw control is provided by the floor turntable. The HARS system is shown in Figures 1.1 and 1.2.

Figure 1.1: HARS system installed in LSWT test section with 55.5-inch sting

Various design modifications have been made to the HARS system to improve functionality since its introduction to the LSWT in 1999. The last such modification was in 2014 in order to improve roll load capacity. The 2014 bullet redesign included a larger roll motor and transmission and a redesigned mounting bracket and transmission fairing at the base of the sting. Since that redesign, several sting-mounted tests have experienced problematic aerodynamic interference. For models with tails located in close proximity to the 10.5-inch diameter bullet, excessive flow deflection around the bullet fairing was suspected to be interfering with aerodynamic data, especially in drag and pitching moment. These findings suggest a redesign is needed to reduce aerodynamic interference and improve data quality.

Figure 1.2: 2014 HARS system installed in LSWT test section

Another data quality improvement is desired that would enable new measurements using the HARS system. In a previous thesis [1], accelerometers attached to a wind tunnel model were intended to provide data for model attitude estimation and dynamical system identification. However, the collected accelerometer data was too noisy to be useful. The cause was determined to be excessive electronic noise of the servo motors actively holding HARS position during testing. The HARS system controls pitch using two AC servo motors that independently drive lead screws in the two struts, and roll is controlled by a servo motor in the bullet. Yaw is controlled by another motor driving the floor turntable. These four motors introduced enough noise to the system that

any accelerometer data from the model was effectively drowned out by the motors actively holding position.

1.2 Objective

The objective of this thesis is to improve aerodynamic data quality of sting-mounted wind tunnel tests by implementing several redesigns to the HARS system. The first goal is to reduce aerodynamic interference caused by the bullet by substantially decreasing its diameter. The diameter reduction must maintain roll-moment and sting-bending-moment capacity. Verification of the aerodynamic improvements to the HARS system includes measuring and comparing measured force and moment data of a 6%-scale, 7.35-ft wingspan NASA WB-57 Canberra aircraft model, as shown in Figure 1.3. This model was tested at the LSWT in 2014 and is now used for aerodynamic engineering course instruction at TAMU. This model was selected for validation purposes because its tail location makes it particularly susceptible to bullet interference from the HARS system when mounted on shorter stings.

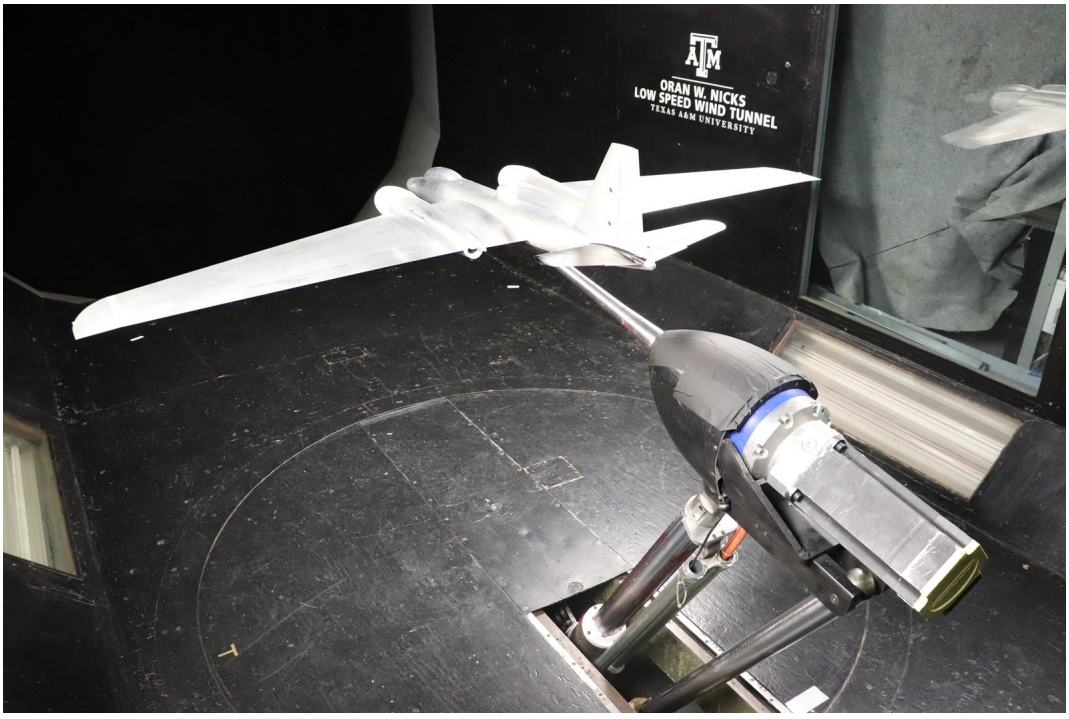

Figure 1.3: WB-57 model mounted to HARS in LSWT test section

In addition to comparing measured balance data of the WB-57 model, particle image velocimetry (PIV) is used to directly measure the amount of flow deflection in two areas upwind of the HARS bullet. These regions over the sting represent the areas where flow is likely impinging on the tail of the WB-57. This will quantify the reduction in flow deflection around the redesigned bullet.

The second goal of this thesis is to reduce electronic noise by replacing all HARS drive motors with motors equipped with passive holding brakes. The AC servo motors that drive pitch, yaw, and roll introduce excessive electronic noise to the system that can interfere with data collection from model-mounted instruments. Motors with passive holding brakes will allow the motors to be programmatically switched off before data is collected while maintaining model position.

These new motors will come with new servo drives that will supply the power and control to the motors and ensure their safe operation. New servo drives will require an updated control software to be able to send the HARS system to its required position. New control software will be written in LabVIEW. It will include a modernized connectivity method over ethernet rather than the outdated method by the current motors, as well as a new interface for controlling the HARS system. This HARS software will also be the start of the LSWT's software overhaul from Visual Basic to LabVIEW.

2. BACKGROUND

2.1 Facility Description

The Low-Speed Wind Tunnel at Texas A&M University has been in operation since its construction in the late 1950s. Its first trial run was performed in November 1958 and its first commercial test was conducted in May 1960. Since that time, the LSWT has been a center for aerodynamic research and education. The LSWT is named for Oran W. Nicks, the tunnel's director from 1980 until his death in 1998. Prior to his time at the LSWT, Nicks served at NASA from 1961-1980 as Director of Lunar and Planetary Programs, Deputy Associate Administrator of Space Science and Applications, Associate Administrator for Advanced Research and Technology, and the Deputy Director of NASA Langley.

The LSWT test section is 14 feet long, 7 feet high, and 10 feet wide with one-foot corner chamfers. Static pressure is maintained near atmospheric pressure with three-inch vents in the side walls at the test section exit. The test section walls diverge about 1 inch over 12 feet to account for boundary layer growth and eliminate streamwise bouyancy.

A 46-ft-long diffuser downstream of the test section provides the transition from the octagonal test section to a 12.5-ft-diameter circular cross section at the power section. The power section consists of a 4-bladed, variable-pitch Curtiss Electric propeller. The propeller is a 15.5-ft-diameter B-29 propeller cut to size for the LSWT. Blade tips are inset into the tunnel wall to minimize tip interference effects. The drive motor is a variable-frequency 3000 hp design by TECO-Westinghouse that can operate up to 1200 RPM. Blade pitch is used as the primary means of speed control.

The 30-ft-long contraction section upstream of the test section transitions from the 30-ft-diameter circular settling chamber to the test section with a contraction ratio of 10.4. Two turbulence screens located just upstream of the contraction provide a uniform inflow and reduce turbulence. Turning vanes are located at each of four 90° turns in the circuit. The facility layout is given in Figure 2.1.

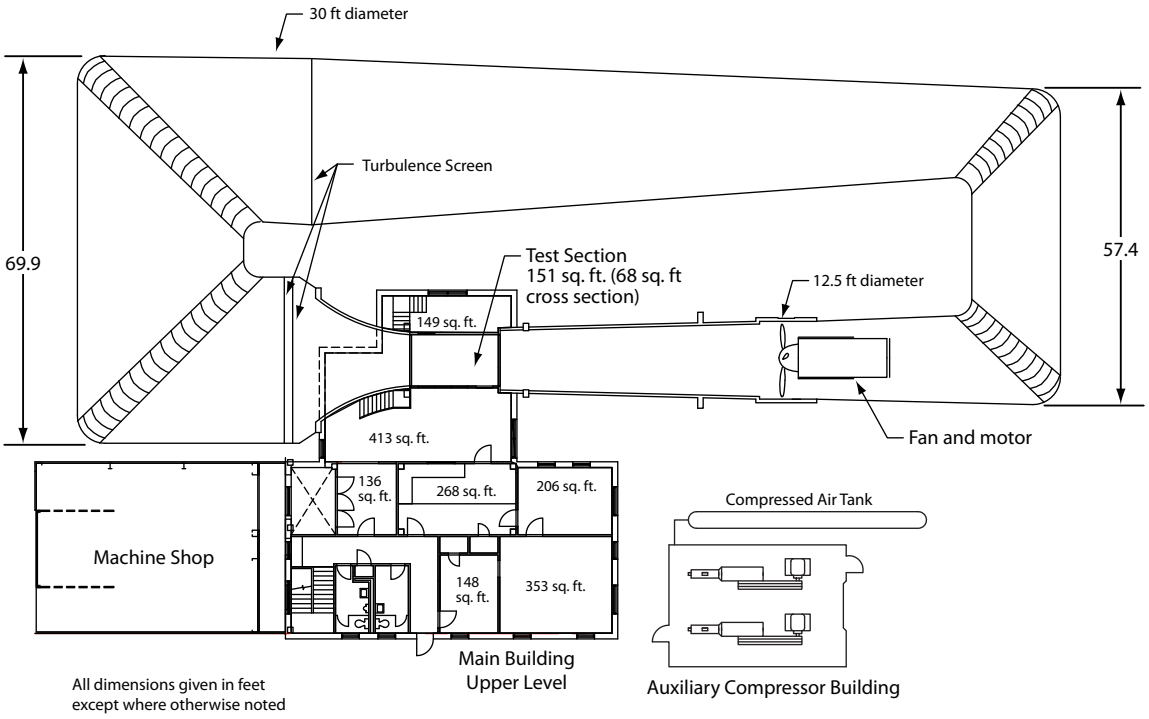

Figure 2.1: Schematic View of the Texas A&M Low Speed Wind Tunnel.

The principle measurement system is a large six-component, pyramidal electromechanical balance located below the test section on the first floor of the facility. The balance resolves aerodynamic forces and moments in a wind-fixed coordinate system with its origin at the geometric center of the test section, 42 inches above the floor on the turntable rotation axis. Force, moment, and attitude measurements are transmitted to the data acquisition system control via optical encoders. The balance turntable yaw range is $-120°$ to $+190°$. Lift force can be measured from -1000 lb_f to $+3000$ lb_f. Drag and side force can be measured from ± 1000 lb_f. Forces are accurate to the greater of 0.25 lb_f or 0.1% of the applied load. Pitching and rolling moments can be measured to ± 2000 ft-lb_f or 0.1% of the applied moment. A variety of support systems are available for mounting models to the external balance. Fairings and image struts are available for tare and interference measurements. More than 300 channels of electronic pressure instrumentation are available as are many additional systems for strain-gauge balances and other instruments. The test section is outfitted with a traversing mechanism for hotwire anemometers or pressure probes.

The HARS system was designed for the LSWT as a removable means of testing sting-mounted models on a mechanism designed to be compatible with the existing external balance infrastructure. For sting-mounted model tests using HARS, a variety of stings and two 1.25-inch diameter internal balances are available. One is a Task Mark X balance capable of measuring 100 lb_f of normal force and 60 lb_f of axial force. The other is a Task Mark XIII capable of measuring 500 lb_f of normal force and 150 lb_f of axial force. The Mark XIII is used for the measurements reported in this thesis, and its limits and uncertainties are shown in Table 2.1. The Mark XIII measures two normal forces, two side forces, axial force, and rolling moment. Pitching and yawing moments are calculated using the two normal and side force measurements respectively.

Normal Force (N1, N2)	500 lb_f, $\pm$0.4 lb_f
Side Force (S1, S2)	500 lb_f, $\pm$0.5 lb_f
Axial Force (AF)	150 lb_f, $\pm$0.1 lb_f
Rolling Moment (RM)	800 in$\cdot lb_f$, $\pm$1.7 in$\cdot lb_f$
Pitching Moment (PM)	2625 in$\cdot lb_f$
Yawing Moment (YM)	2125 in$\cdot lb_f$

Table 2.1: Mark XIII internal balance limits and measurement uncertainties.

2.2 Previous HARS Design Changes

The HARS system has been through three major design changes since its introduction in 1999. The first redesign in 2009, shown in Figure 2.2, was the first major overhaul of the system. This redesign introduced the struts that are still in use today and reconfigured much of the sting mount bullet assembly, as well as the strut drive components such as motors and transmissions. Model pitch is driven by ACME lead screws located in the two struts. Each strut is driven by an AC servo motor with a 22:1 transmission and the strut lead screws at 5 turns/inch of extension.

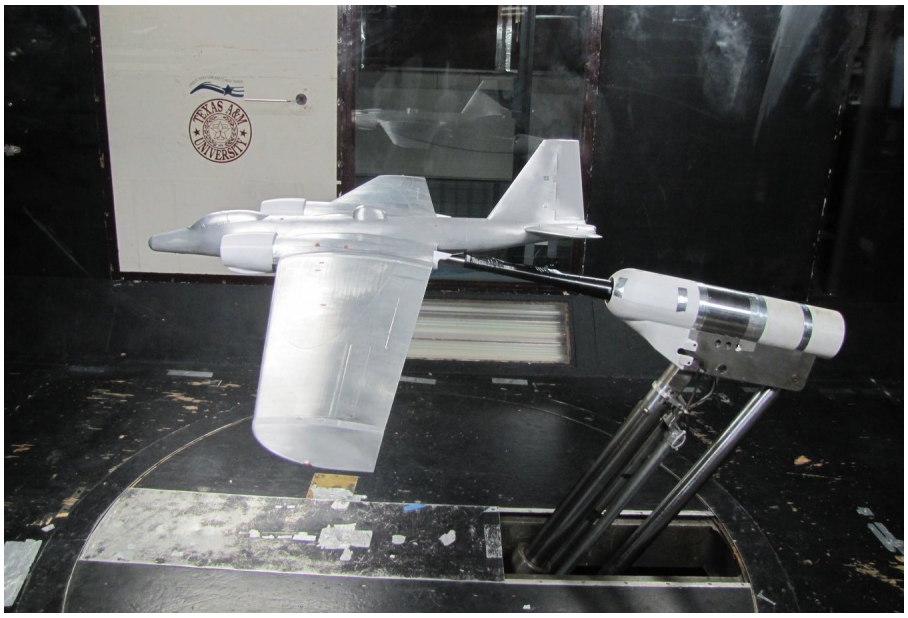

Figure 2.2: 2009 HARS system installed in LSWT test section with WB-57 model

The 2009 bullet design used two angular contact ball bearings with an intermediate shaft to withstand sting root bending moments. The shaft connected the sting mounting base to the roll transmission, a Carson Mfg. Inc. 40:1 planetary gearset capable of a max output torque of 1963 in·lb_f, powered by a Baldor DSMS34F-3B stepper motor. This bullet design experienced frequent stepper motor overheating issues. Due to a complicated design both to assemble and manufacture, it was difficult to adapt different drive components.

To expand sting-mounted testing capabilities, an alternative to mounting models directly to the sting is a sting balance block offset called the blade, shown in Figure 2.3. With the blade installed, the internal balance is located 1.0 ft from the sting axis. This means the motor and transmission must be capable of withstanding the rolling moment of the model in addition to the moment generated by the balance side force times that offset distance. The 2009 design's transmission and motor combination was unable to produce enough torque to reliably hold the model with the blade installed. Because this version of HARS could not be easily retrofitted with a more capable motor and transmission, the roll system was completely redesigned in 2014.

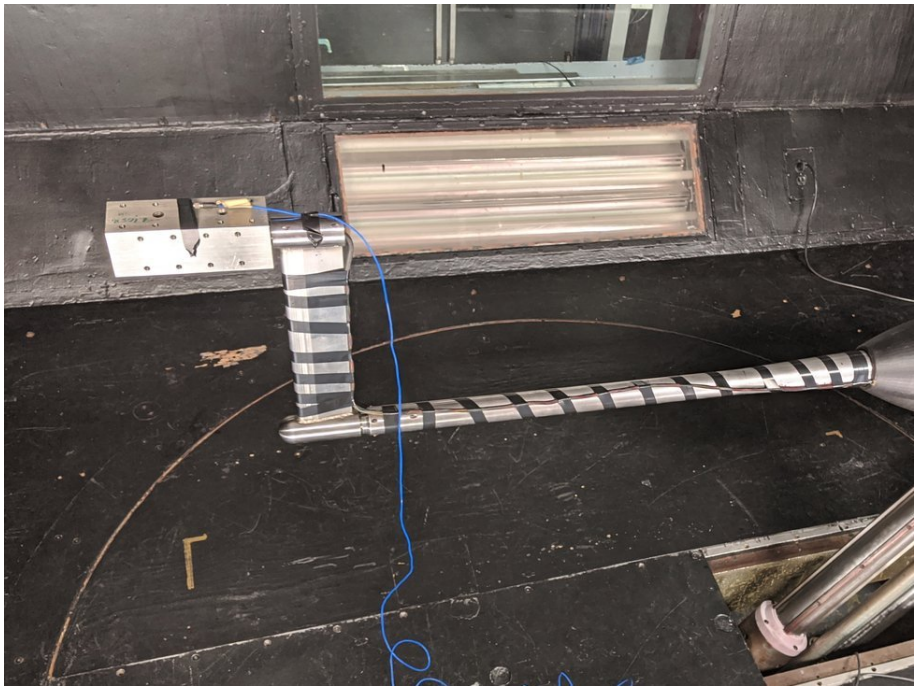

Figure 2.3: Blade and balance block installed on a sting

The 2014 redesign, which is the implementation the work in this thesis will replace, features a roll motor and transmission with a much higher torque and load capacity than the 2009 system. This design, shown in Figure 2.4, opted not to use bearings and an intermediate shaft to bear the root bending moment of the sting. Instead, the gear reduction transmission from the roll motor

to the sting was selected such that the sting bending moment could be withstood directly by the transmission. This resulted in selecting the Wittenstein TP 110S 70:1 planetary gearbox capable of withstanding a maximum root bending moment of 29,030 in·lb_f with a nominal maximum roll torque of 7966 in·lb_f, coupled to a Baldor BSM100N AC servo motor.

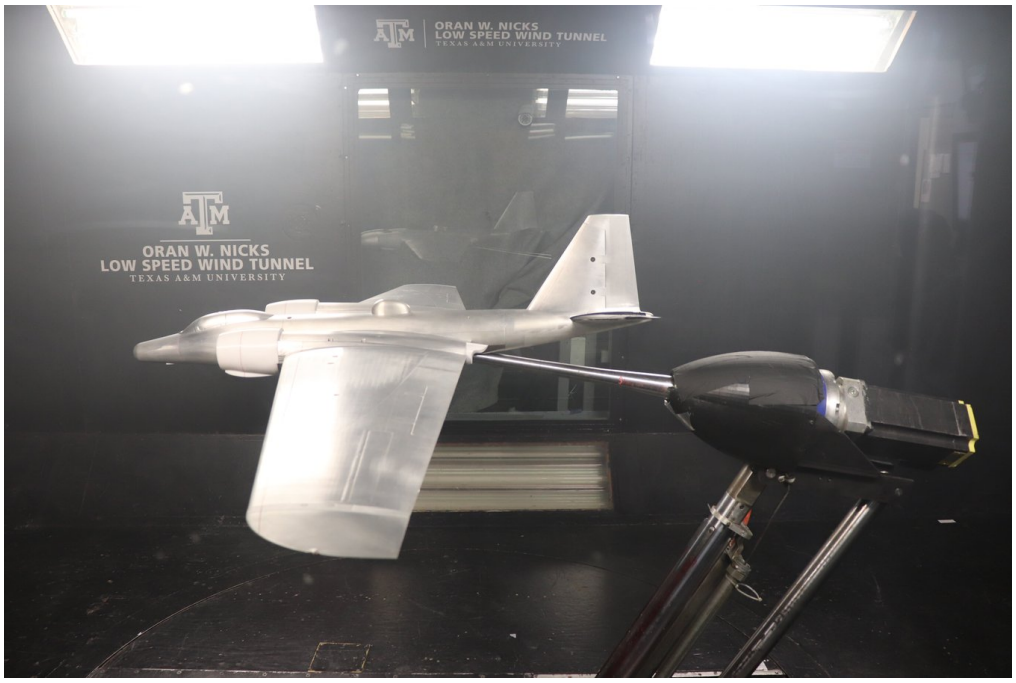

Figure 2.4: 2014 HARS system installed in LSWT test section with WB-57 model

This design is capable of withstanding any sting bending moment that may be encountered in testing and significantly exceeds the 800 in·lb_f rolling moment limit of the internal balance when mounted on the blade. In addition, the 2014 design is capable of accommodating blade-mounted models at any pitch angle up to 90°. As a result, this transmission is over 10 inches in diameter. This large diameter is suspected to be the cause of excessive aerodynamic interference.

2.3 HARS System Problems to Address

In several sting-mounted tests where the aft end of the model was in close proximity to the bullet, the internal balance data showed trends that were not expected for the given model. For ex-

ample, some models with tails close to the model showed larger than expected nose-down pitching moments that did not follow expected trends over the tested range of pitch angles. This could result from HARS-induced upflow around the bullet. The obvious solution would be to install models on a longer sting farther away from the bullet. However, for heavier models or models that show extreme dynamic behavior at or near stall, the aerodynamic-induced oscillations that can occur are substantially worsened by installing on a longer sting. The WB-57 model used in this thesis is one such model. This makes time-averaged data collection difficult. Worse still, extreme dynamic loads can be detrimental to internal balance strain gauge longevity. Therefore, it is more desirable to test models on shorter stings to mitigate some of these model oscillations.

To decrease the flow deflection around the HARS bullet, an entirely new transmission and mounting bracket assembly will need to be selected and designed to replace the current system. This will reduce flow deflection around the HARS bullet thereby reducing aerodynamic interference around the model. With the method the 2014 design utilized to withstand the root bending moment of the sting, it will not be enough to simply replace the transmission with a smaller one; the entire sting mounting system will have to be rethought in order to operate safely with a smaller transmission.

Regarding especially dynamic models, such as the WB-57 that this thesis will use for verification purposes, it is desired to be able to measure pitch-induced stall oscillations through the use of model-mounted accelerometers as shown in Figure 2.5. This was attempted by Cratty in 2017 [1], but the collected accelerometer data was heavily contaminated by electronic noise introduced to the system by the AC servo motors that drive and control HARS attitude and position. Due to the excessive noise by these motors, collecting useful accelerometer data is nearly impossible. In addition, these motors introduce enough noise to affect the collected internal balance data, which could also degrade data quality. This is evident in Figure 2.6 when comparing the collected internal balance and accelerometer data between having the motors in normal operating condition and turning the motors off completely.

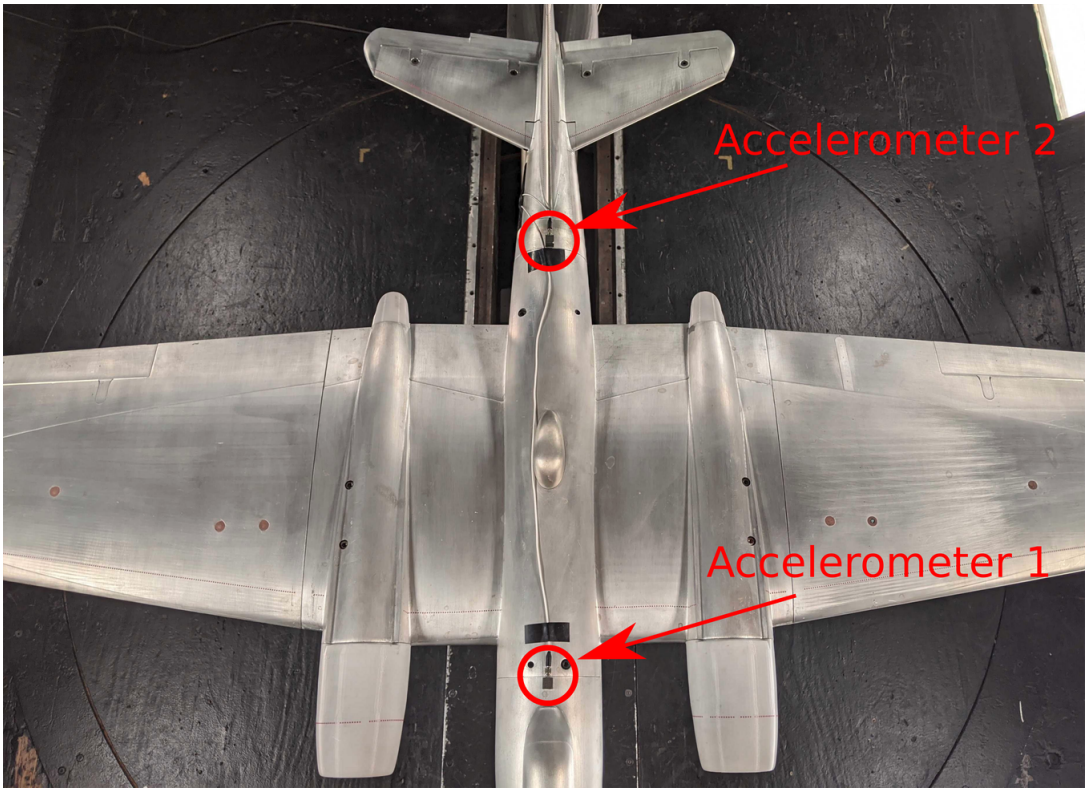

Figure 2.5: Accelerometers installed on WB-57 model

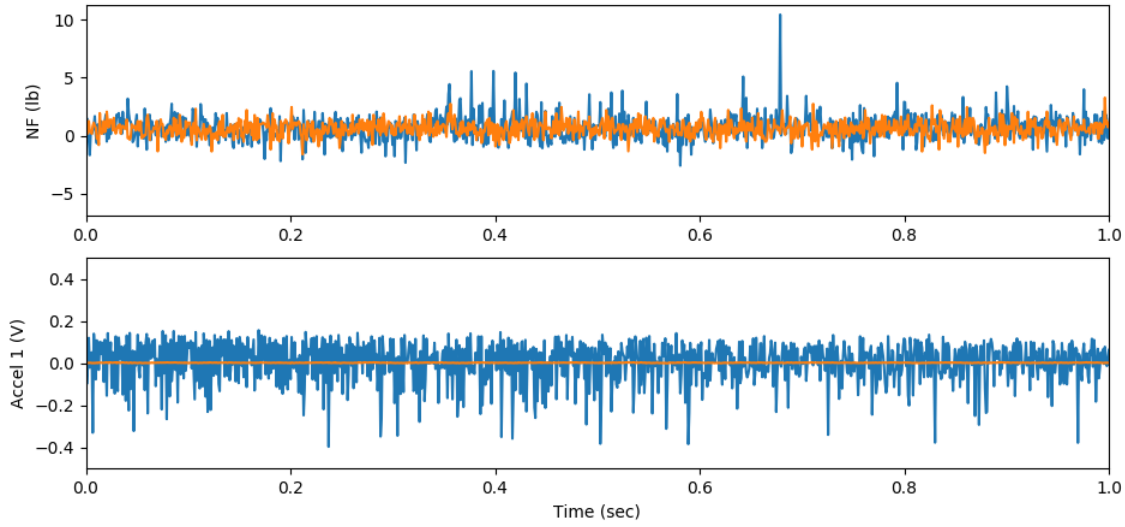

Figure 2.6: Internal balance strain gauge normal force and accelerometer readings with no wind. Blue shows system motors enabled, orange is system motors disabled.

In addition to the excessive noise and flow deflection, this system has additional problems that are commonly encountered in testing. For the past few years, the HARS system has sporadically been incapable of performing roll attitude adjustments due to various problems with the outdated servo motor, drive system, and software. The HARS system has instead been operated with a roll system lockout plate in place of the roll motor when tests do not require roll position changes. However, this has introduced several needless limitations to sting-mounted tests.

The problems arising from the HARS roll system were among the first hints that major system modification was needed to continue proper utilization of the HARS system. The current servo motor drive system includes three Baldor FlexDrive II servo drives running two BSM80N servo motors for the struts, and a BSM100N servo motor for the roll system. In addition to the HARS system itself, another Baldor Flexdrive II servo drive and BSM80N motor is used to rotate the floor turntable. These drives and motors are controlled via the control software written in Visual Basic (VB), communicating through a Baldor-proprietary PCI card, 100-pin cable, and servo drive breakout boards. The hardware in use is outdated by over 15 years, with no ability for service or replacements should drives or motors fail. In addition, the VB motion control software written in 2009 requires out-of-date software drivers, and few future or current LSWT staff are familiar with VB in case code modifications become necessary.

3. HARS DESIGN CHANGES

To address the issues encountered by the current HARS system, two major design changes will be implemented. The HARS bullet, which includes the roll system, mounting bracket, and sting mounting base, will be completely redesigned to reduce its overall cross-sectional area. This will reduce the blockage caused by the HARS bullet and reduce flow deflection. The second change to the implemented is the complete replacement of all servo motor and drive components. To eliminate electronic noise, motors with passive holding brakes will be installed, and a new control software will be developed to drive these motors.

3.1 Proposed Design Changes & Constraints

The primary change to be considered in the HARS redesign is the reduction of the overall diameter of the bullet assembly. The connecting flange of the roll motor transmission is the foremost determinant of the diameter of the bullet, so the transmission selected must be smaller while maintaining sufficient torque to hold and drive the sting within a reasonable factor of safety. Holding torque is the capability of the system to hold attitude against aerodynamic loads, and driving torque is the additional capacity to drive roll against aerodynamic loads.

The redesigned bullet assembly must be capable of utilizing the sting mounting hardware currently in use so that only as many parts as necessary will be redesigned and machined. Therefore the redesigned bullet must be capable of mating with the existing sting mount adapter. In addition to the sting mounting hardware, the bullet mounting bracket must be compatible with the existing struts, with the additional design constraint that the bullet must be capable of reaching a pitch angle of 90° vertically.

The materials and components to be used were selected to withstand any aerodynamic forces and moments encountered by a model during wind tunnel testing. As a baseline, the limits of the Mark XIII internal balance were used to determine the maximum static forces and moments the bullet assembly must be capable of withstanding. Since the internal balance is monitored

such that its limits are never exceeded, the upper normal force and pitching moment limits of the balance while mounted to the longest used sting in the LSWT inventory were used to determine the maximum root bending moment experienced by the bullet. A free body diagram showing the resultant root bending moment at the bearings is shown in Figure 3.1. The bearings will act as a moment couple to withstand the resultant sting bending moment, each responsible for the total moment load divided by the distance between the two bearings.

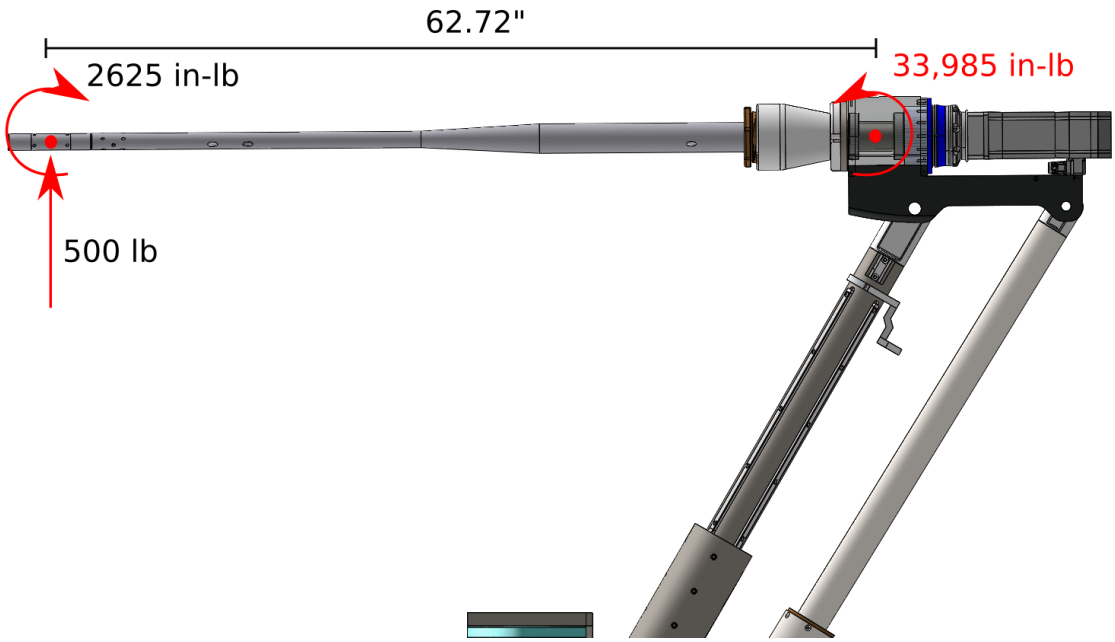

Figure 3.1: Free-Body Diagram of HARS resultant moment from maximum-loaded internal balance on 55.5-inch sting.

In addition to reducing the overall diameter of the bullet, the AC servo motors that drive position of the HARS system are desired to be replaced with motors that are equipped with passive holding brakes. In its current state, the motors drive the two struts and roll to position and must actively maintain its position. Because these motors are constantly on and driving the struts, a large amount of electric and mechanical noise is introduced to the system. This noise is suspected to be interfering with internal balance readings which is undesirable. Additionally, this noise tends

to contaminate other measurements such as readings from accelerometers.

As the existing strut and roll motors have been in use since 2009 and earlier, much of the motor hardware is outdated, including the AC servo drives, control software, and the AC servo motors themselves. The servo drives in use for the two strut motors, the roll motor, and the floor turntable are Baldor Flexdrive II drives that are unsupported and discontinued by the manufacturer (as well as ABB, the company that subsequently bought and rebranded Baldor). The drives are connected to the LSWT Motion Control computer using a 100 pin cable connected to a proprietary NVME card. The software used to drive the system was written in 2009 using Microsoft Visual Basic Studio, and few LSWT personnel have the knowledge to effectively modify this code. Therefore, to use a modern servo drive system, an updated control software must also be written as part of this work.

3.2 Components Selected

The new redesign of the HARS bullet returns to an approach similar to the 2009 design, implementing two bearings and an intermediate shaft to withstand the sting bending moment. This allows the transmission to be solely responsible for delivering roll torque through a shaft connecting the transmission to the sting base. The shaft was machined of stainless steel that provides high strength and corrosion resistance. On each end of the shaft are flanges that mate with the sting adapter and transmission.

With the loads determined, and the bearings set at 3.44 inches apart, each bearing must be capable of withstanding nearly 10,000 lb_f of normal load. The bearings selected are two SFK NUP 210 ECP cylindrical roller bearings, each rated for a normal static load of 15,624 lb_f [2]. These two bearings are interference-fitted into the steel bearing block. Roller bearings were selected over the previously-used angular contact ball bearings because the HARS system is predominantly a static system, holding the sting where the bearings will be in one rotational position over a long enough period of time to collect a data sample. Cylindrical roller bearings distribute the static load over a line rather than a point and will cause less wear on the bearing race.

The new transmission selected is a Wittenstein TP025S High Torque 154:1 planetary gearbox

capable of an output torque of 4647 in·lb_f. This is coupled to a Nidec Unimotor HD AC servo motor with a passive holding brake. This new motor and transmission combination is capable of holding up to 6000 in·lb_f of roll torque without introducing additional noise to the system. The new transmission is 5.7 inches in diameter and, including the new bullet fairing, allows a maximum bullet diameter of 6.0 inches.

The front fairing was designed so that the circular cross section of the sting smoothly transitions to the shape of the mounting bracket while minimizing internal volume around the sting adapter with a streamlined shape. The rear fairing continues the cross-sectional area of the steel bearing block and is secured in the aft end of the mounting bracket. The bullet fairings were manufactured at the LSWT out of rapid-prototype polycarbinate (PC) in the LSWT's Stratasys FDM 400MC 3D printer. CAD images of the redesigned bullet are shown in Figures 3.2 and 3.3 and the completed HARS bullet with plastic fairings is shown in Figure 3.4.

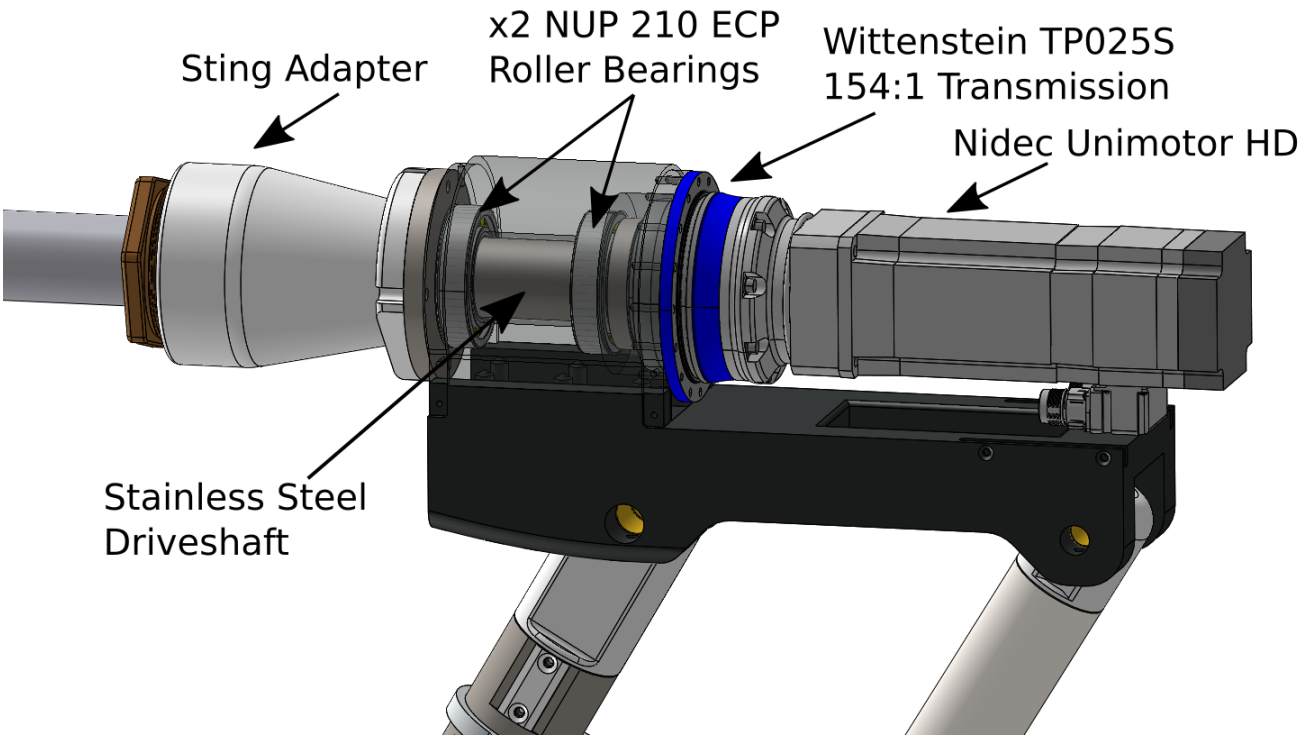

Figure 3.2: CAD model of redesigned HARS bullet, plastic fairings not shown.

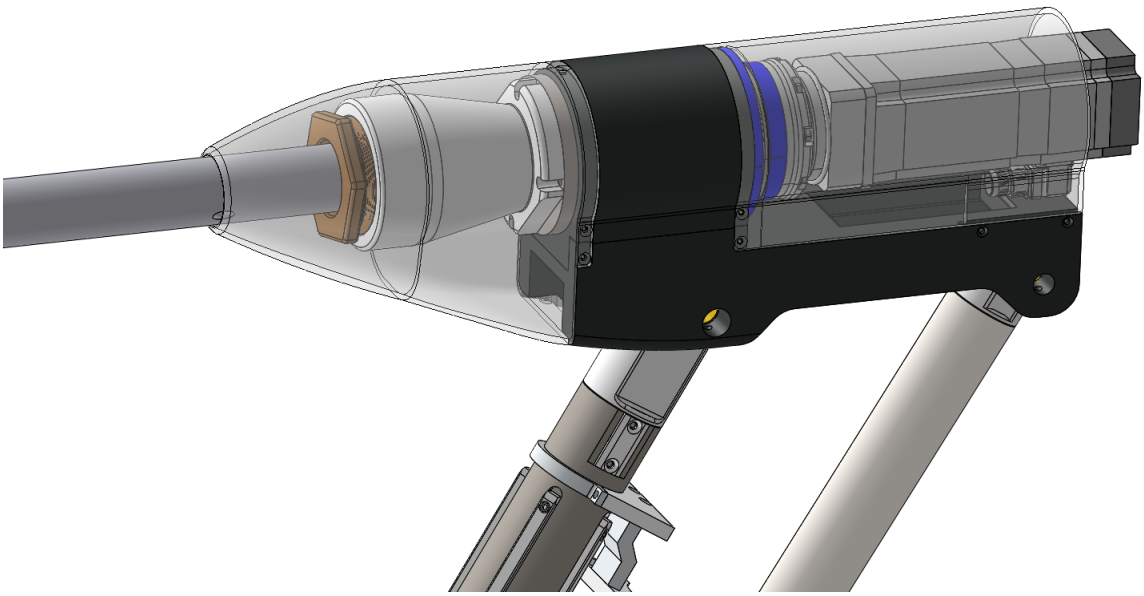

Figure 3.3: CAD model of redesigned HARS bullet, plastic fairings shown.

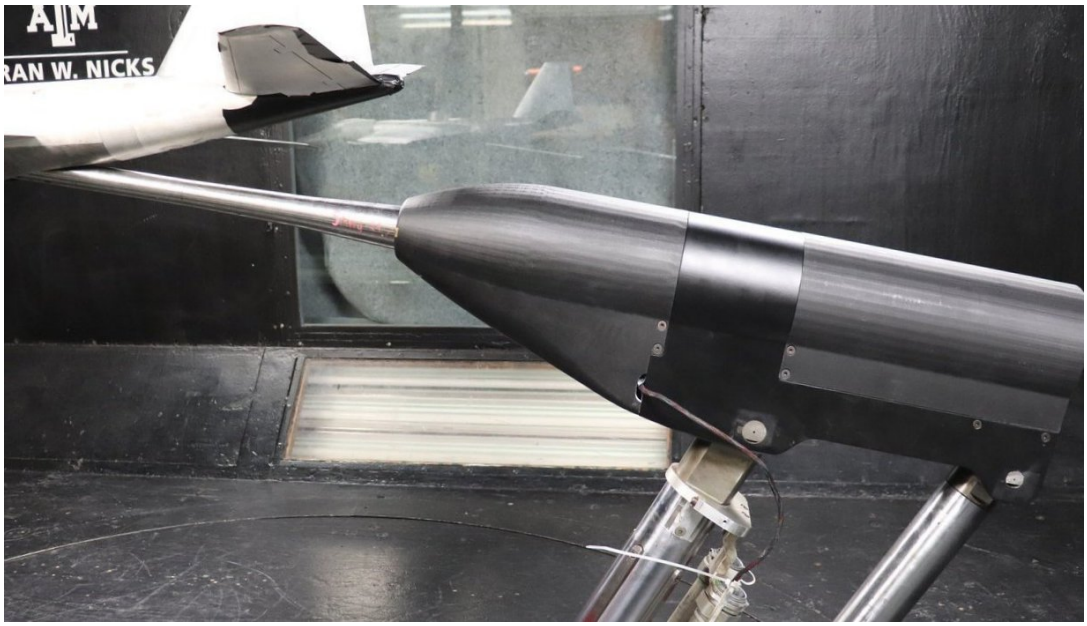

Figure 3.4: Redesigned HARS bullet completed and installed in LSWT test section

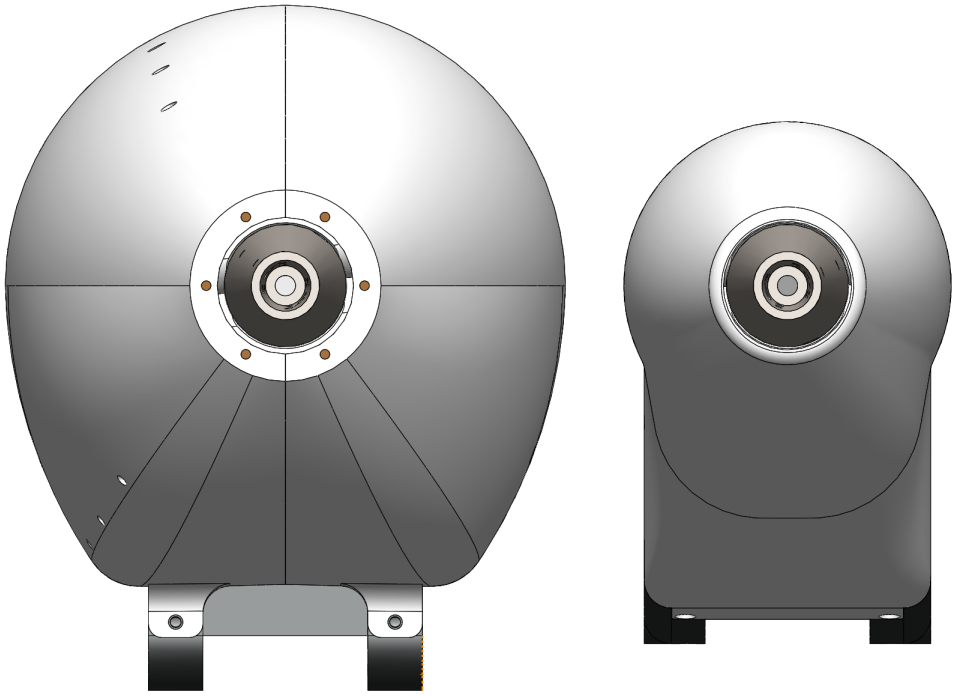

Figure 3.5: 2014 HARS bullet diameter compared to redesigned bullet

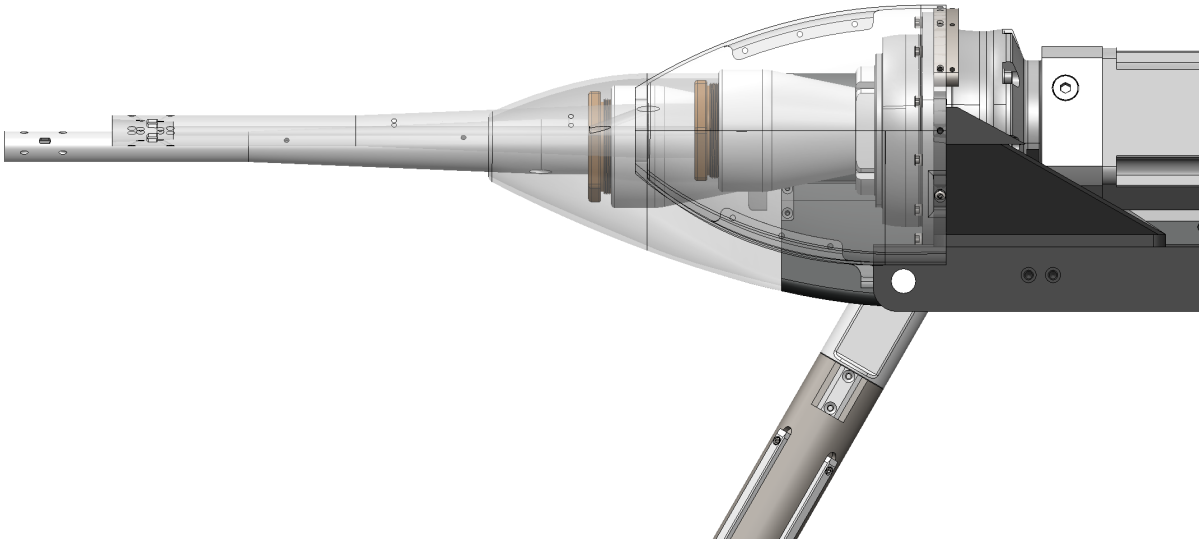

Figure 3.6: Sting base located 4.4 inches more forward of the front strut than 2014 bullet

The new structure and drive components were selected to be capable of withstanding the maximum possible normal force and pitching moment measurable by the Mark XIII internal balance when mounted on the longest used sting in the LSWT inventory. The new system can withstand loads of 500 lb_f normal and 2625 $in \cdot lb_f$ pitching moment simultaneously applied at the end of a 55.5-inch sting. This exceeds any realistic aerodynamic load to be experienced by the system. Additionally, the redesigned bullet is capable of withstanding a maximum of 500 lb_f of side force measured by the balance when mounted to the blade that provides a 12-inch roll moment arm.

The roll transmission and motor are capable of holding position and driving against any expected aerodynamic roll moment load in most configurations. With the blade installed, the HARS roll motor would only need to provide holding torque via the brake. The roll motor would not be engaged and any test with the blade installed would involve pitch and yaw sweeps, not pitch and roll sweeps. Driving roll with the blade installed was a design requirement of the previous version of HARS, partly owing to the bullet's larger size. However, that requirement was determined to no longer be necessary for this redesign.

The AC servo motor drives selected for the roll motor and the two strut motors (identical to the roll motor) are three Nidec Epsilon EP servo drives by Control Techniques. These drives are capable of being daisychained and controlled via a single ethernet cable connected to the LSWT Motion Control computer. To control these drives, a new software was written in LabVIEW, communicating to the drives via Modbus TCP protocol. This new control software is the start of the LSWT's control software overhaul from Visual Basic to LabVIEW.

4. PERFORMANCE VERIFICATION

Several tests were conducted to verify the data quality improvements provided by the HARS modifications. It is suspected that the 10.5-inch bullet fairing of the 2014 HARS design resulted in excessive flow deflection around the aft end of sting-mounted models, so particle image velocimetry (PIV) was used to directly measure the upwards flow deflection around the bullet fairing. Reducing the flow deflection of the HARS bullet is expected to show a difference in aerodynamic balance data, primarily in the longitudinal axis of the model. If the redesigned bullet decreases the upwards flow deflection at the tail, the balance data should reflect a more positive pitching moment about the model moment center in addition to other effects in lift and drag. Finally, internal balance data and accelerometer data were compared before and after the new motors were installed to verify the reduction in noise and quality of collected data.

4.1 Bullet Flow Deflection PIV

Particle image velocimetry was used to measure the flow field upstream of the HARS system at 0° pitch and 0° yaw for the 2014 bullet and the redesigned bullet without the WB-57 model installed. In each case, the PIV measurement plane was aligned in the test section x-z plane to measure the streamwise/vertical velocities (u, w) above the centerline of the sting. The PIV measurement system consisted of a New Wave Solo 120 Nd-YAG laser (12-mJ per 3-5 ns pulse at 532 nm), a Cooke Corp PCO 1600 14-bit interline transfer camera (70 dB dynamic range) with a Nikon 70-300 mm lens, miscellaneous optics, and an 8-channel Quantum Composer Model 9618 pulse generator to control timing of the laser and camera. The flow was seeded with a MDG Max 5000 Fog Generator, which produces 10,000 ft^3/min of 500-700 nm diameter particles. Analysis was performed using LaVision's DaVis processing software. [3]

Before installing the redesigned HARS bullet to the struts, PIV data was collected on the 2014 HARS bullet fairing for analysis. However, inconsistencies in collected PIV data due to measurement errors and excessive reflections obstructing the flow region resulted in the initial PIV data

unable to be effectively analyzed. Because the previously installed 2014 HARS bullet could not be easily reinstalled (and then subsequently the redesigned system reinstalled), an alternative method was devised so representative PIV data could be collected and compared. The 2014 bullet fairing design was printed using a Stratasys FDM 400MC 3D printer and designed to be compatible with the redesigned bullet assembly to facilitate PIV testing, as shown in Figure 4.1. That is, PIV comparisons are between the bullet fairing designs of the 2014 HARS bullet that is 10.5 inches in diameter and the redesigned bullet, both mounted on the redesigned HARS bullet assembly. Black tape was applied to the sting and bullet fairing to reduce reflections of the PIV laser interfering with data collection.

Figure 4.1: 2014 bullet fairing installed on new HARS bullet for PIV data capture

The regions captured by the PIV system were 5.2 $\times$ 4.8 inches in size and located two inches above the centerline of the sting. Two regions over the sting and forward of the bullet were chosen to be close to where flow was likely impinging on the tail of the WB-57 model. The PIV results of

the flow deflection is shown in Figures 4.2 & 4.3.

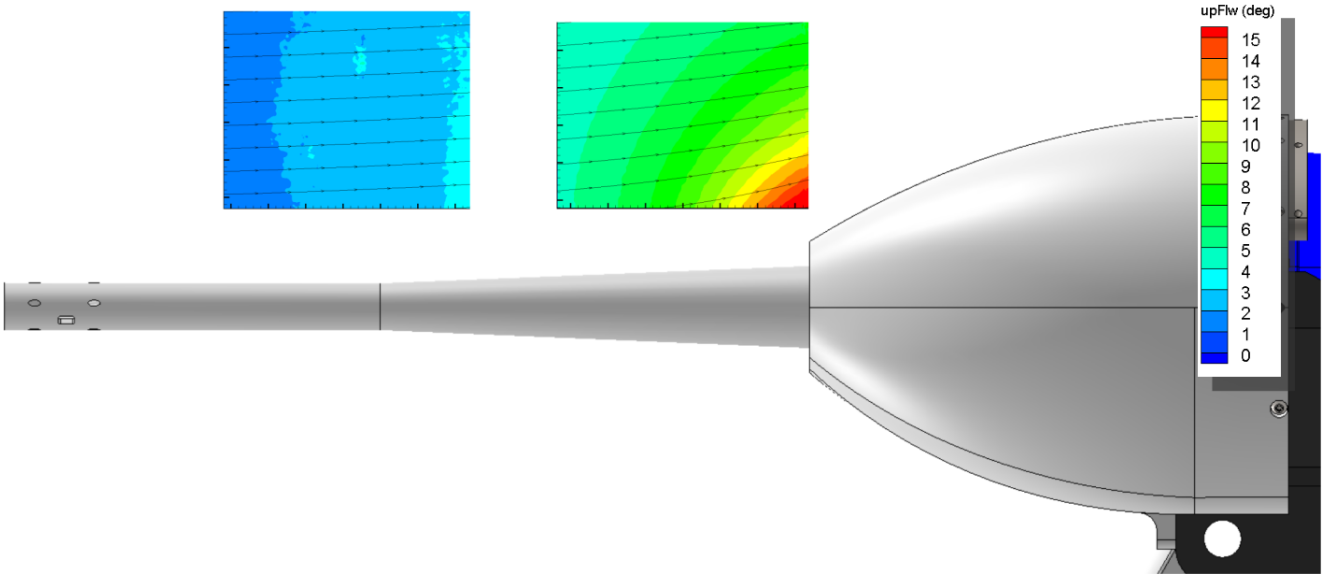

Figure 4.2: 2014 bullet fairing PIV flow deflection results

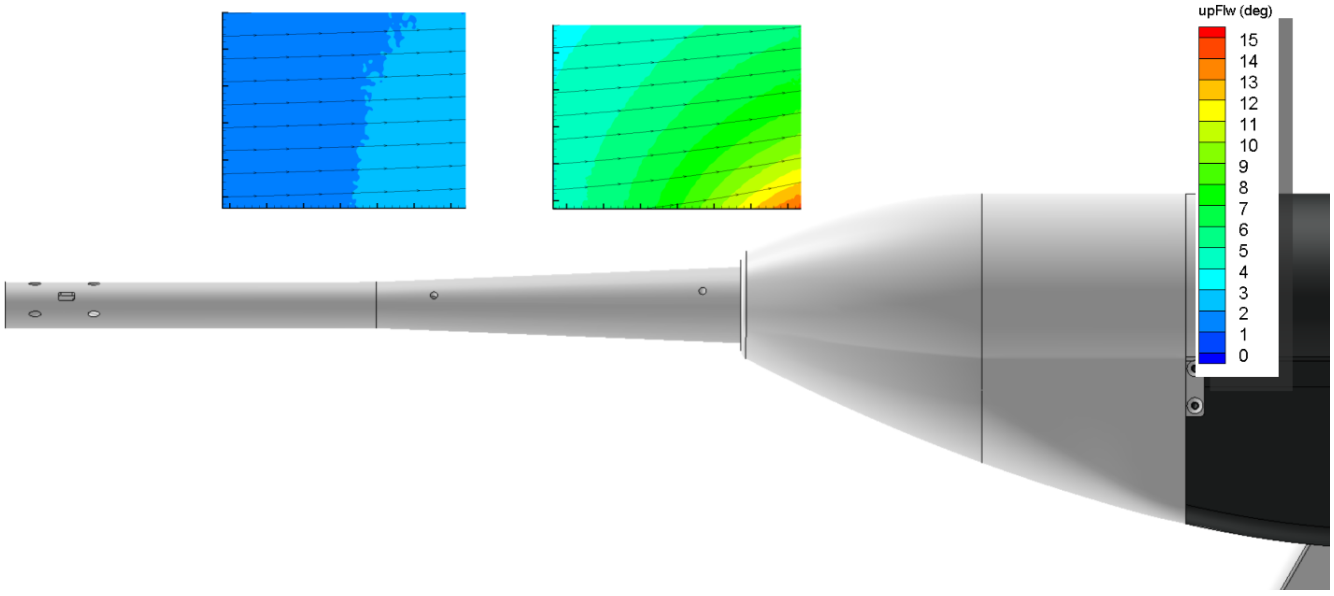

Figure 4.3: Redesigned bullet fairing PIV flow deflection results

These results show a clear decrease in flow deflection at both locations upstream of the bullet fairing. In particular, the flow is deflected 2°-3° less near the region where the WB-57 tail is located with the redesigned bullet fairing. Because lifting surfaces are very sensitive to inflow angle, the lessened flow deflection behind the model will have a substantial impact on the aerodynamic data due to the reduced upflow at the tail.

4.2 Aerodynamic Data

Internal balance data for the WB-57 model was collected and analyzed for differences between the 2014 HARS bullet design (the entire assembly, not just the fairing) and the redesigned bullet. Aerodynamic force and moment data was obtained using the Mark XIII internal balance. The sting and balance penetrate the WB-57 model 10° from the aircraft waterline, so balance loads are rotated by 10° to yield body-frame data and again by aircraft angle of attack to yield wind-frame data.

The testing procedure included angle of attack sweeps at $\beta = 0°$ at a speed of 50 mph or a dynamic pressure of approximately $q = 6.4$ psf. After static tare loads were subtracted, the nondimensionalized load data of the WB-57 aircraft model were compared mounted to both the 2014 HARS bullet and the redesigned bullet. Lift, drag, and pitch moment data were analyzed for differences between the two systems. The data is nondimensionalized into lift, drag, and pitching moment coefficients, C_L, C_D, and C_m, using the wing planform area of 7.2 ft^2 and a reference chord length of 1.045 ft. Pitching moments were taken about the internal balance moment center then transferred to a moment reference center 4.41 inches forward and 1.60 inches above the balance moment center in the model-fixed frame.

4.2.1 Corrections Applied

In typical wind-tunnel testing, various corrections are applied to the force and moment data to best approximate free-air performance. Several effects of testing in a closed test section have to be accounted for such as solid blockage, wake blockage, streamwise bouyancy, and other effects. Since the interest of this testing is to assess the effects of the mounting system itself and not the

model in question, only essential load corrections were applied.

The first correction applied to the load data accounts for the deflection of the sting under aerodynamic loads. Sting deflection causes the model angle of attack to differ from the commanded angle of attack position set by HARS by an amount proportional to the normal force. The sting deflection is measured by incrementally loading weights to the end of the sting and measuring the deflection using a dial indicator. The sting deflection is well approximated as a linear correlation to the normal load applied. For the 29.75-inch sting used in this test, the sting deflection correction is 0.0065° per lb_f normal force. For data reduction, the angle of attack of a test point is increased in magnitude by this constant multiplied by the measured normal force.

In addition to frame rotations and sting bending corrections, the second correction applied to the measured data are corrections for upflow in the test section due to the model support system. The overall blockage of the new design is less than the previous design, so a new upflow angle must be determined. This is done by measuring the lift of the model as a function of angle of attack through a pitch sweep both upright (0° roll) and inverted (180° roll). The offset between the $C_L(\alpha)$ data of the upright and inverted configurations is twice the upflow angle [4]. The configurations tested are shown in Figure 4.4 with the model mounted to the 29.75-inch sting on the redesigned system.

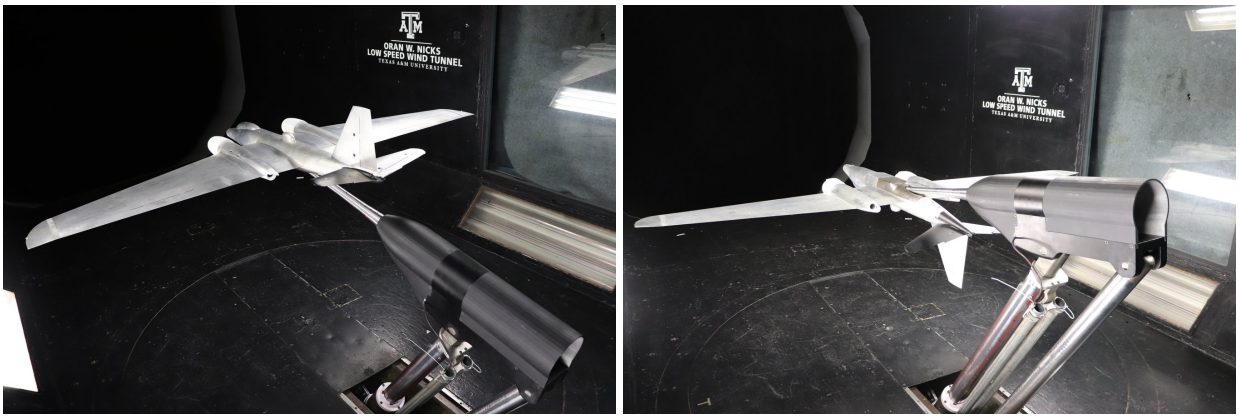

Figure 4.4: WB-57 upflow test on the redesigned system, upright and inverted

Upflow angle was determined for both the 2014 HARS bullet and the redesigned system as shown in Figure 4.5. The upflow angle was calculated from the $\alpha < 0°$ data due to the loss of linearity of the inverted data above 0° angle of attack. This is likely due to the proximity of the model to the wind tunnel floor and HARS struts. Results show the 2014 design produces 0.76° of upflow while the redesigned system produces 0.53°, about 1/3 less.

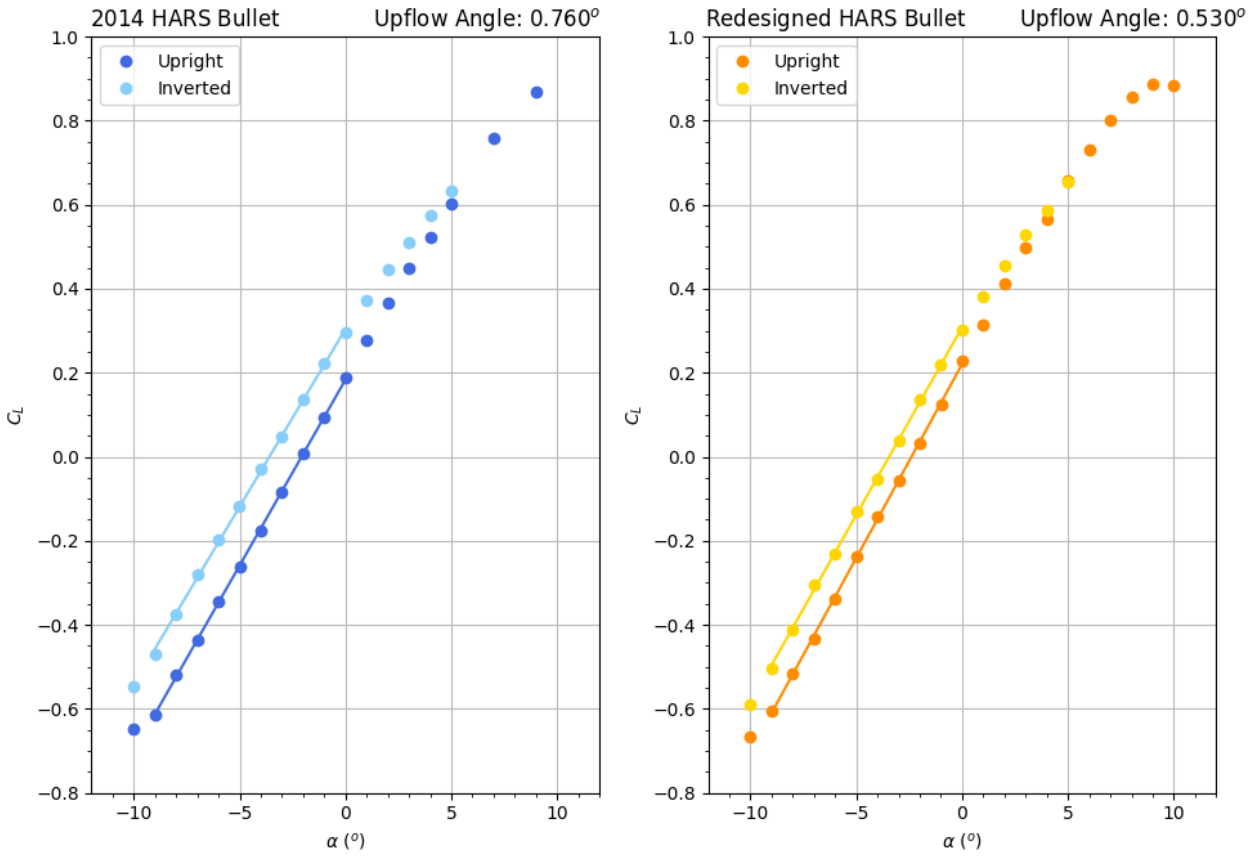

Figure 4.5: Upflow angle comparison. Left: 2014 HARS with 0.78° upflow. Right: current redesign with 0.53° upflow.

While reducing bullet diameter was the principle aim of the redesign, it is not thought to be the reason for the reduced upflow. Instead, the new design locates the base of the sting more forward in the test section away from the struts which are likely to be the main contributor to the upflow

(see Figure 3.6). This is useful because it enables shorter stings that exhibit lower amounts of sting deflection to be used while maintaining flow quality around the model with less upflow correction. Regardless of the reason, the reduced upflow angle is evidence of a successful redesign that reduces the aerodynamic interference due to the HARS system.

4.2.2 Load Data Analysis

The load comparison of the WB-57 model using the 2014 and redesigned systems were performed using the 29.75-inch sting. Internal balance data was collected from pitch sweeps of -10° to 15° at $q = 6.4$ psf or approximately 50 mph. The lift, drag, and pitching moment data were then nondimensionalized and sting deflection and upflow angle corrections were applied at each data point. After applying the two corrections, the lift and pitching moment load data are plotted against the corrected angle of attack, and a drag polar $C_L(C_D)$ was plotted. These results are shown in Figures 4.6, 4.7, and 4.8.

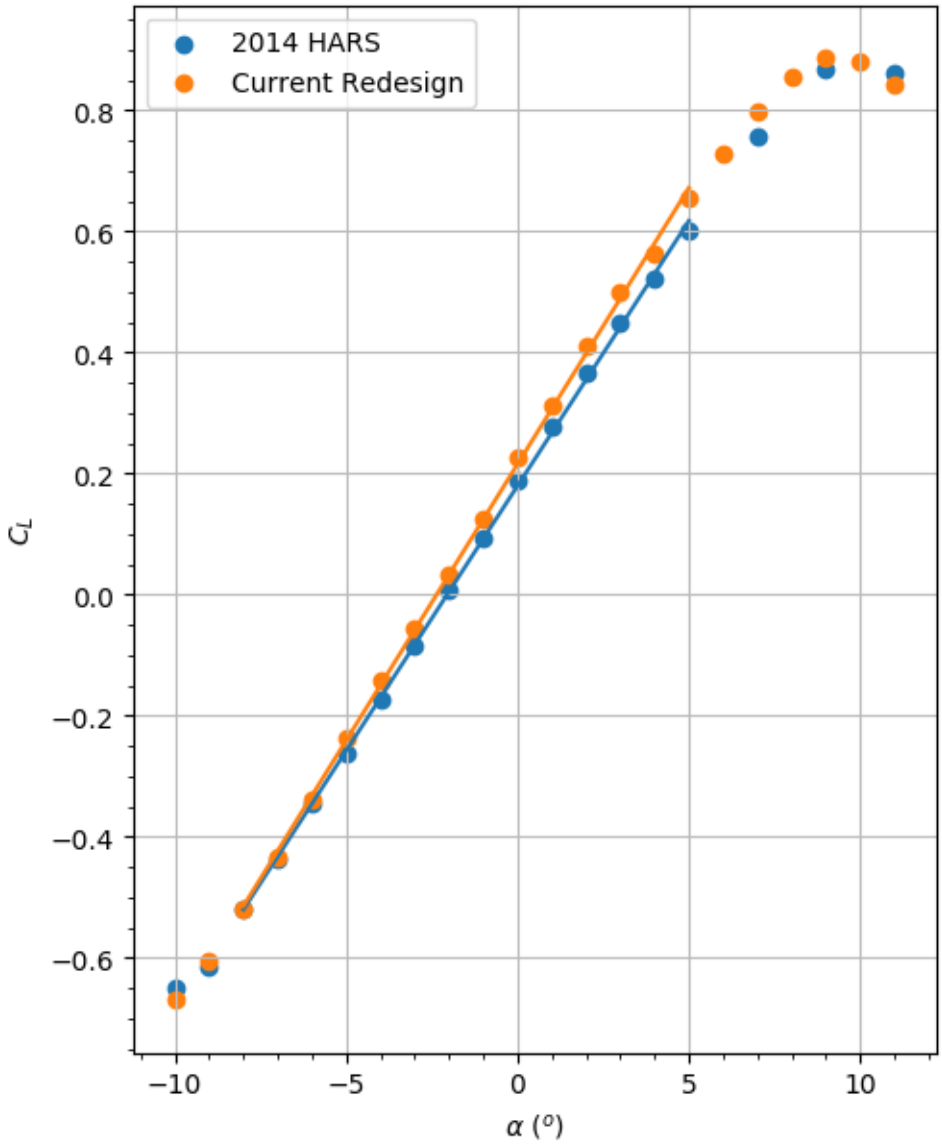

Figure 4.6: Comparison of lift $C_L(\alpha)$ results of the 2014 and redesigned systems. Linear fit applied between -8° and 5°.

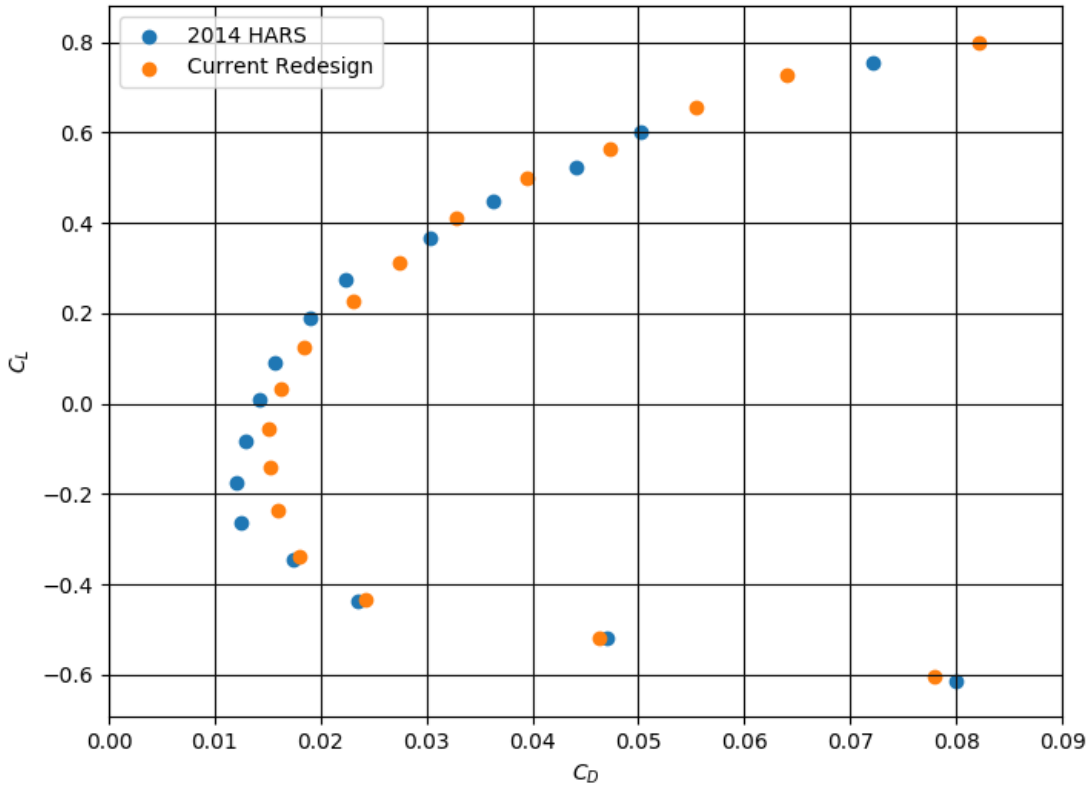

Figure 4.7: Comparison of the 2014 and redesigned systems' drag polars $C_L(C_D)$.

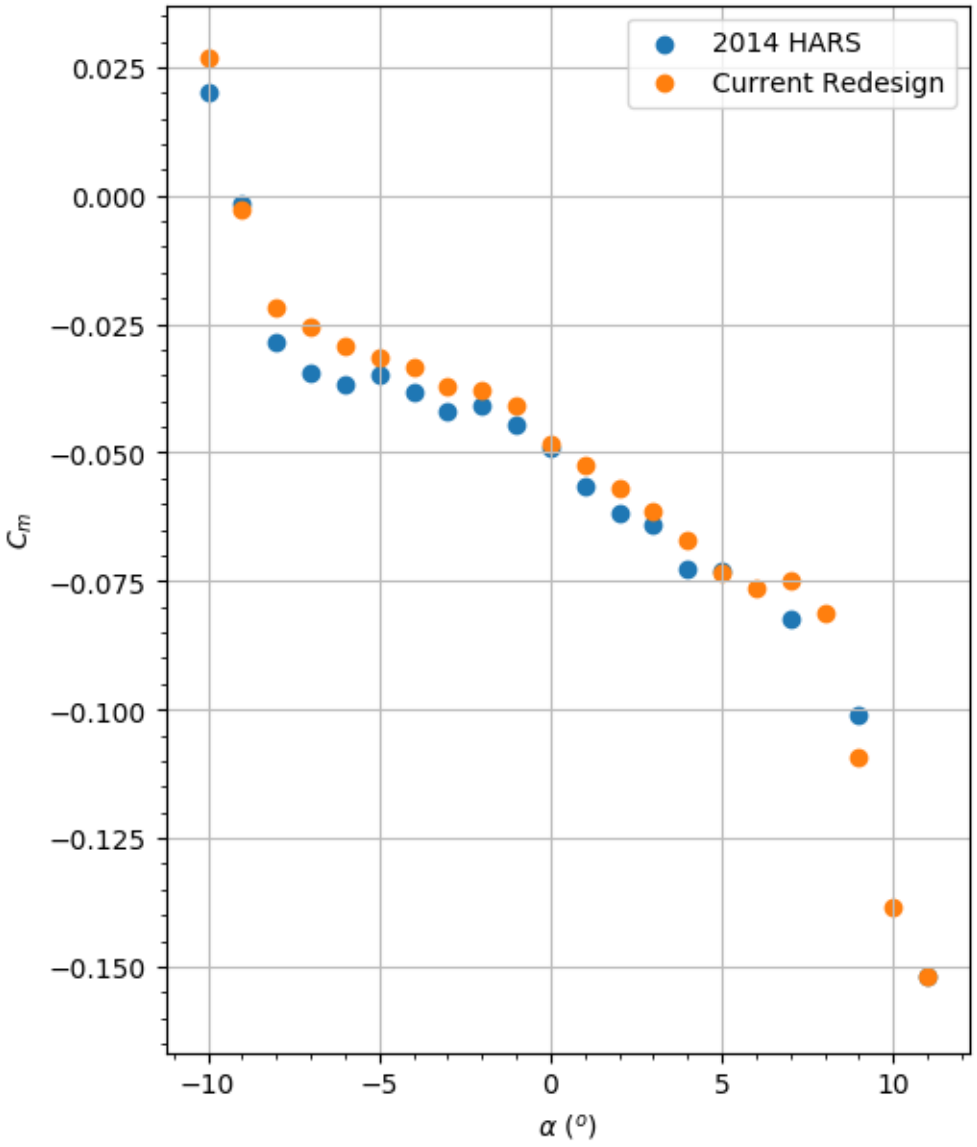

Figure 4.8: Comparison of pitching moment $C_m(\alpha)$ results of the 2014 and redesigned systems

It is observed in Figure 4.6 that the slopes of the $C_L(\alpha)$ curves differ slightly between the two bullet designs. A linear fit was applied to the data between $\alpha = -8^\circ$ to $\alpha = 5^\circ$ and it was found that $dC_L/d\alpha$ of the current redesign is 5.228 ± 0.038 per radian from the 5.014 ± 0.029 per radian as measured for the previous design. Additionally, the zero-lift angle of attack $\alpha_{L=0}$ was found to decrease from the $-2.05^\circ \pm 0.01^\circ$ for the 2014 HARS bullet to $-2.36^\circ \pm 0.02^\circ$ for the current redesign. Uncertainty calculations are provided in Appendix B.

As originally expected, Figure 4.8 shows that the pitching moment is somewhat less negative (less nose-down) for the current redesign. This would result from weaker HARS-induced upflow at the tail which would lead to an artificially large negative pitch moment. This result shows that the redesigned bullet exhibits less upwards flow deflection at the tail than the previous design. In addition to reducing upflow at the tail over the full range of α, the upflow is dramatically decreased at the region of $\alpha < -2^\circ$ as shown by the greater increase in C_m. In this angle of attack range, the HARS bullet rises more behind the WB-57 tail as the model pitches downwards, causing even greater upflow at the tail. The current redesign shows an improvement in the consistency of the measurement, as evidenced by the improved linearity of the $C_m(\alpha)$ of the current redesign.

4.3 Accelerometer Data Analysis

Up to this point, all data has been collected using the old Baldor strut motors that actively hold the HARS position. By replacing these motors with the Nidec motors with passive holding brakes, electrical noise will be reduced or eliminated while maintaining the ability to accurately hold HARS position. To quantify the reduction in noise from the motors, tests were conducted using two accelerometers by PCB Piezoelectronics attached to the WB-57 model before and after the motors were replaced. Internal balance data and accelerometer data were collected for both static and wind-on tests to verify that usable data can be collected. These tests collected data over a range of four seconds at a sampling frequency of 1024 Hz. The two accelerometers were attached along the longitudinal axis of the model as shown in Figure 4.9.

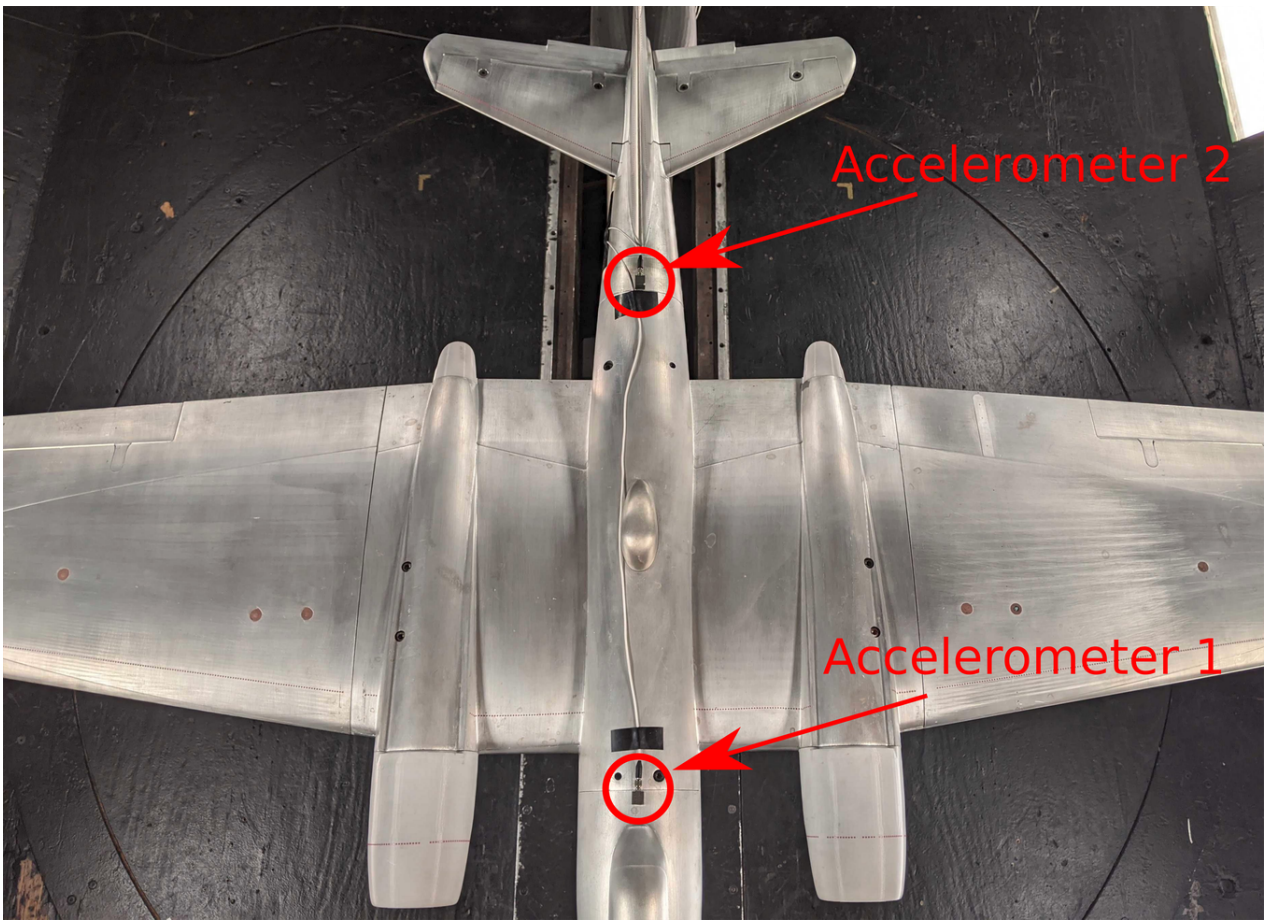

Figure 4.9: Two accelerometers attached to the top of the WB-57 model.

	Model Number	Serial Number	Sensitivity (mV/g)	Bias Level (V)
Accelerometer 1 (A1)	333B40	47712	490	11.1
Accelerometer 2 (A2)	333B40	40733	498	10.9

Table 4.1: Accelerometer specifications and technical data. [6]

The primary challenge that Cratty faced in her work on state estimation using these accelerometers in a similar configuration was the overwhelming noise due to the HARS system motors holding position [1]. The vibration produced by the motors could be felt to the touch and the accelerometers are extremely sensitive to this vibration. For a single wind-off data point, the difference is clear. Figure 4.10 shows how much the vibration of the motors affected the collected accelerometer data.

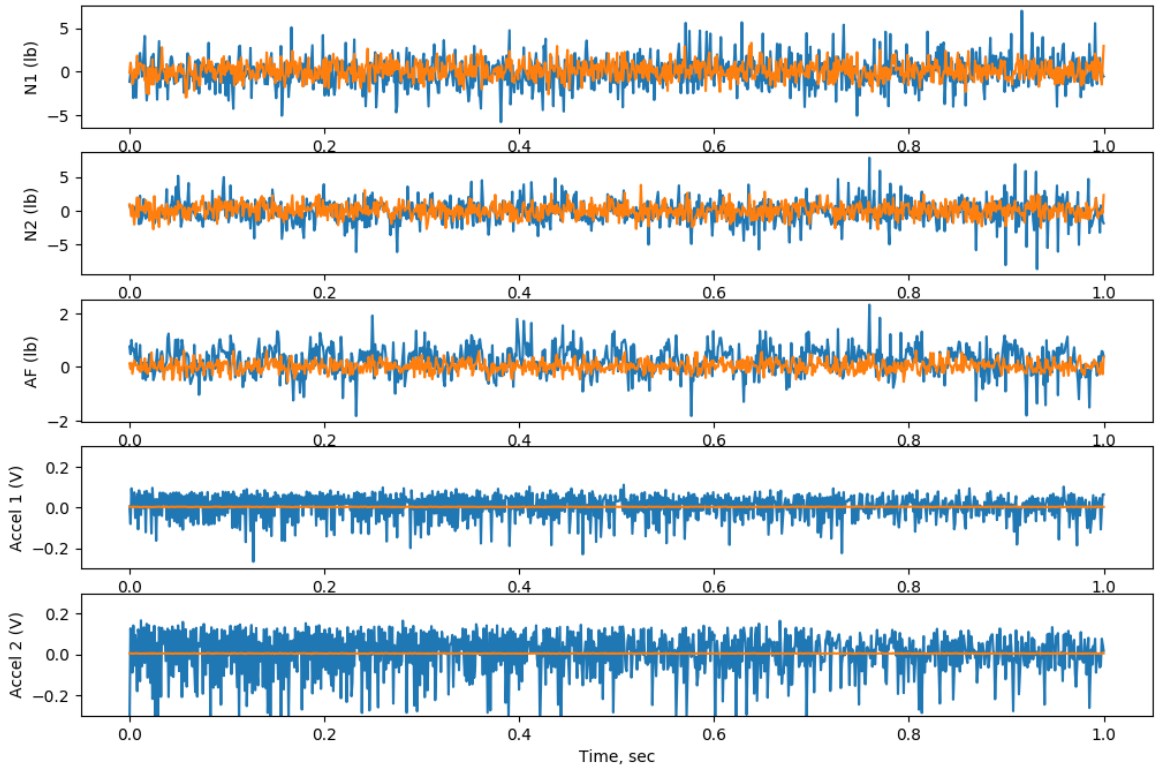

Figure 4.10: Internal balance strain gauge and accelerometer readings during wind-off data point. Blue shows old motors actively holding position. Orange is new motors with passive brakes applied.

	Old Motors	New Motors	New/Old
N1 (lb)	1.206	0.706	0.585
N2 (lb)	1.136	0.745	0.656
Y1 (lb)	1.038	0.748	0.721
Y2 (lb)	1.089	0.741	0.680
RM (in-lb)	1.451	0.962	0.663
AF (lb)	0.348	0.141	0.405
A1 (g)	0.159	0.00144	0.009
A2 (g)	0.232	0.00175	0.008

Table 4.2: Difference in standard deviation between old and new motors

There is a dramatic improvement to the quality of data collected by the two accelerometers. The accelerometers show a flat signal as they should when the model is completely static. The rms noise level with the new motors is less than 1% of the previous value. Additionally, the six internal balance strain gauge channels show a clear improvement as well due to the reduction in noise. The implications of this improvement are that more sensitive measurement instrumentation can now be used on sting-mounted models.

As an example of when accelerometers could be useful, the WB-57 exhibits stall-induced sting oscillations that can be measured by the accelerometers. At a dynamic pressure of $q = 20$ psf, internal balance and accelerometer data were taken the same manner as before, both before and after the motors were replaced. The results for pre-stall condition at $\alpha = 0^\circ$ is shown in Figure 4.12 and post-stall at $\alpha = 12^\circ$ is shown in Figure 4.12. At both conditions, but especially before stall when the model motion is less, the new arrangement is dramatically improved. These changes now enable the system identification work attempted by Cratty [1].

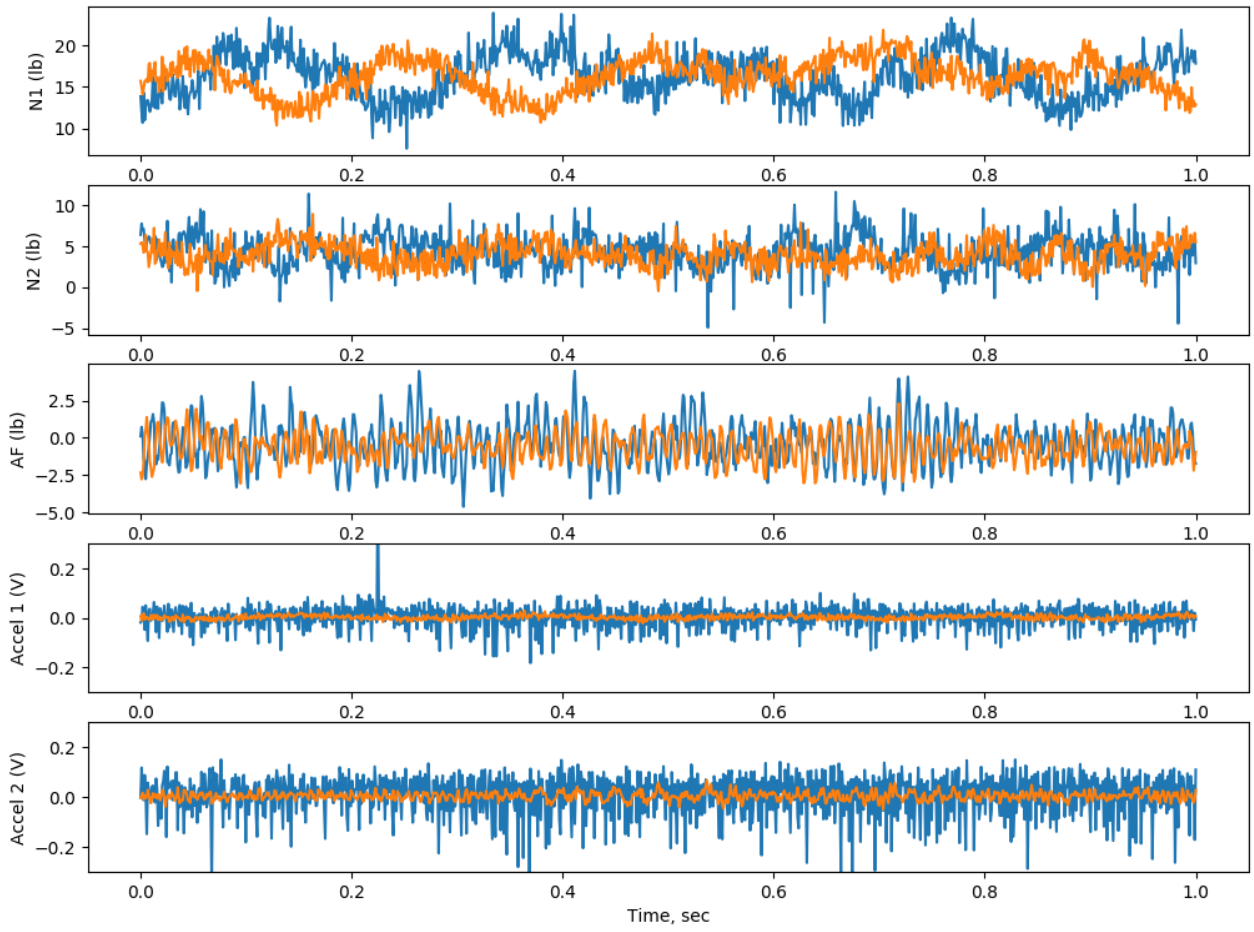

Figure 4.11: Internal balance strain gauge and accelerometer readings at $q = 20$ psf and $\alpha = 0°$ (pre-stall condition). Blue shows old motors and orange is new motors.

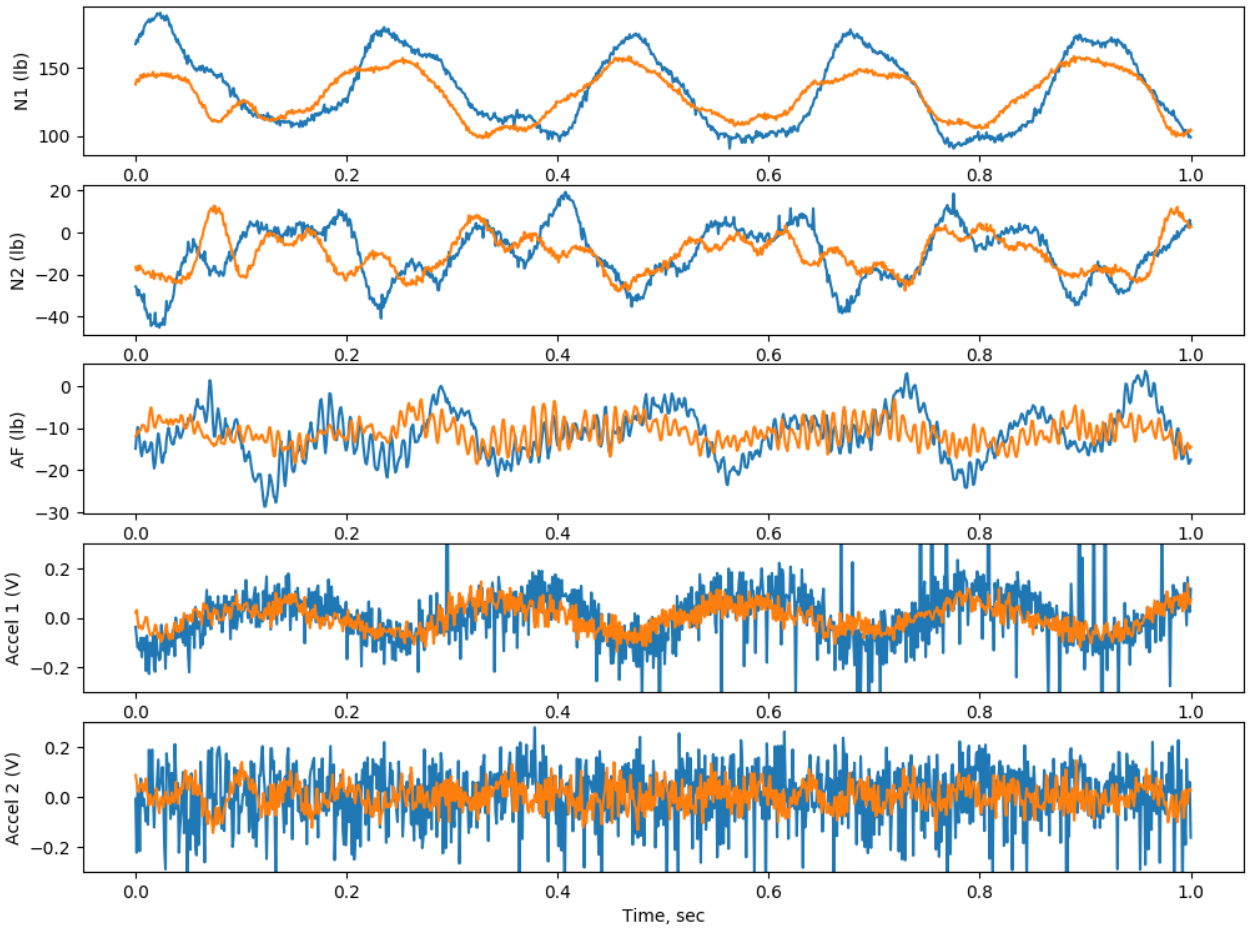

Figure 4.12: Internal balance strain gauge and accelerometer readings at $q = 20$ psf and $\alpha = 12°$ (post-stall condition). Blue shows old motors and orange is new motors.

To further document the improved signal quality, a Fourier transform is applied to the accelerometer signals to yield fluctuation power spectra. Runs at $\alpha = 0°$ and $\alpha = 12°$ are shown in Figures 4.13 and 4.14, respectively. After replacing the motors, the total amplitudes of the accelerometers' signals across the spectrum are reduced by approximately an order of magnitude. This shows that the total noise introduced to the system by the previous motors has been drastically reduced.

It is apparent that prior to the motor replacement, the signal is dominated by a series of peaks associated with the motors holding position. After replacing the motors, clear frequencies representative of the system dynamics are able to be observed. Most notable are the low-frequency oscillations of the WB-57 model bouncing on the sting from Accelerometer 1 and some higher frequency modes of oscillation from Accelerometer 2.

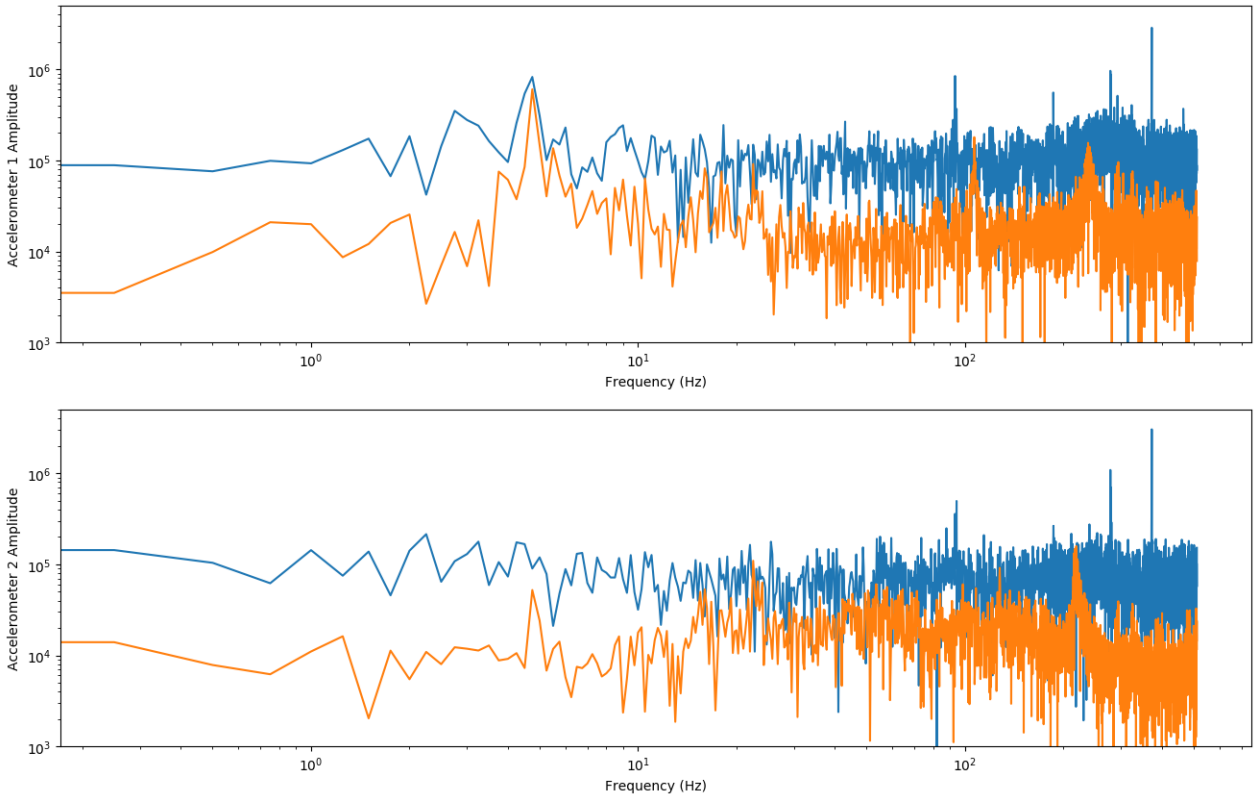

Figure 4.13: Fourier transform of pre-stall condition accelerometer outputs shown in Figure 4.11. Blue shows old motors and orange is new motors.

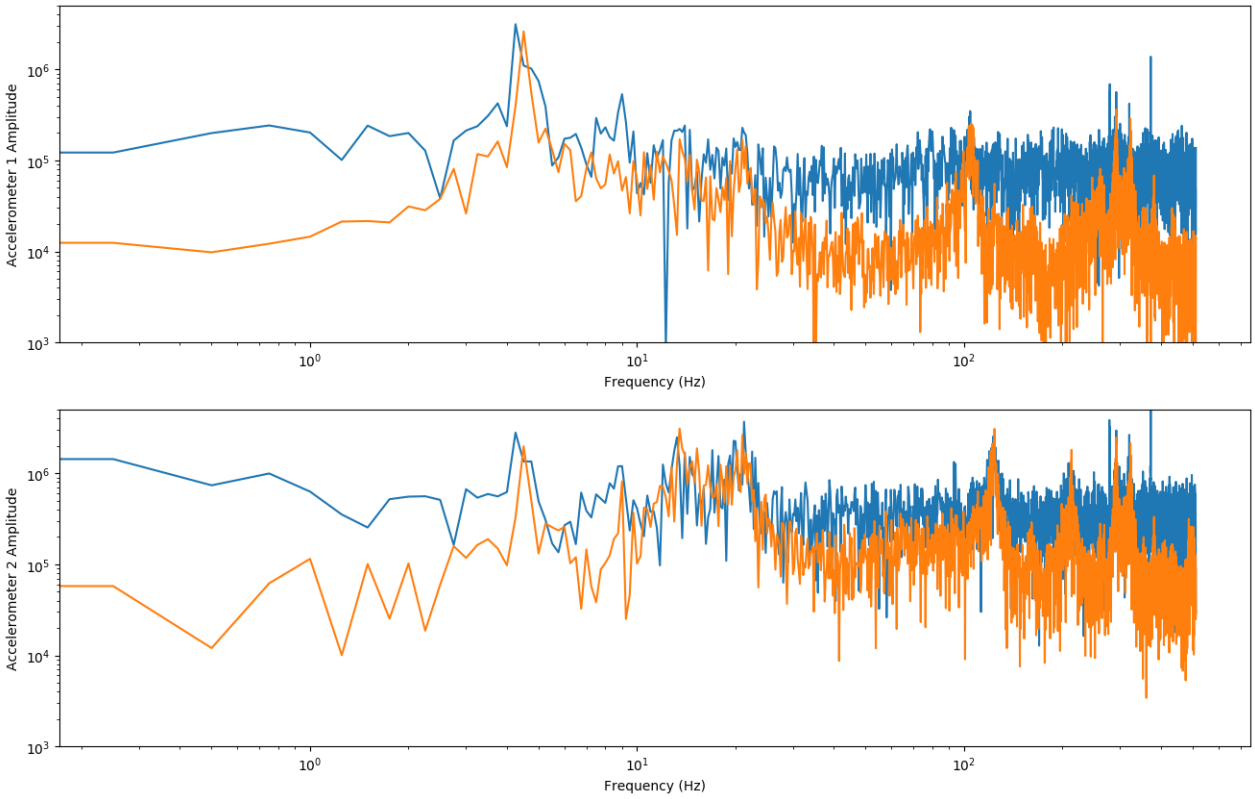

Figure 4.14: Fourier transform of post-stall accelerometer outputs shown in Figure 4.12. Blue shows old motors and orange is new motors.

5. CONCLUSION

The HARS system is the pitch and roll actuator used by the LSWT to test sting-mounted models. Previous implementations of the HARS bullet design and drive components produced excessive aerodynamic and electrical interference to data collection instrumentation. The objectives of this thesis were to redesign the HARS bullet to reduce aerodynamic interference and modernize the drive system with motors that are capable of powering off while maintaining accurate position in the test section.

The redesigned HARS bullet assembly has been shown to have successfully met these objectives. As such, it represents an important improvement in LSWT testing capabilities. The PIV and aerodynamic tests show a clear improvement for the new system due to reduced flow deflection around the bullet. Replacing the drive motors as well has shown a dramatic improvement in the quality of collected accelerometer data, as well as a slight improvement to internal balance aerodynamic data. The new drive system will provide a much quieter electronic environment that will enable testing using more sensitive instruments and this will broaden the capabilities of future sting-mounted tests.

The goal for this thesis was achieved in successfully implementing design changes to the HARS system for improved data quality. The ideal wind tunnel mounting system has zero impact on a tested model, however this ideal cannot be achieved with conventional mounting arrangements. Given the difference in results to aerodynamic data between the old and new HARS bullets, interference of the mounting system in place has been meaningfully reduced. Although it is impossible to know the "truth", it is safe to surmise that the performance data more likely resembles that of the actual aircraft.

REFERENCES

[1] K. M. Cratty, "Dynamic Wind Tunnel Load and Attitude Measurements Using State Estimation," master's thesis, Texas A&M University, 2017.

[2] SKF, *NUP 210 ECP*, 2021. Technical Specification: Cylindrical roller bearings, single row.

[3] E. J. Leber, "Development and Implementation of Piv Systems With Selective Particle Seeding for Production Wind Tunnel Testing," master's thesis, Texas A&M University, 2020.

[4] J. Barlow, W. Rae, and A. Pope, *Low-Speed Wind Tunnel Testing*. Wiley, 1999.

[5] J. John D. Anderson, *Fundamentals of Aerodynamics*. McGraw-Hill, 5 ed., 2011.

[6] PCB Piezoelectronics, 3425 Walden Ave, Depew, NY 14043, *ICP Accelerometer*, g ed., Apr. 2012.

APPENDIX A

RUN LOGS

OWN - LSWT Test 1927
16-19 August 2019

A1 = 5:5:15, A2 = 5:1:15, A3 = 13:2:25, A4 = 0:1:10, A5 = 0:1:25, A6 = -16:2:24, A7 = -16:2:-6
A8 = -6:2:10, A9 = 10:2:16, A10 = -6:2:16, A13 = 4:2:16, A_inv = 0:1:-15
B1 = -14:2:14, B2 = -10:2:10

Run Number	Vel (mph)	Pitch (°)	Yaw (°)	Roll (°)	Static Tare Run Number	Configuration Code	Comments
1	0	A1	0	0	N/A	WB_oldHARS_29.75	Static Tare
2	50	A1	0	0	1	WB_oldHARS_29.75	taking balance data, fouling between PIV points
3	50	A2	0	0	8	WB_oldHARS_29.75	^, finer alpha sweep; gaffer tape on sting
4	50	A3	0	0	8	WB_oldHARS_29.75	^, upper range of alphas
5	50	10	B1	0	8	WB_oldHARS_29.75	Beta sweep, just balance data, 0 degrees alpha
6	50	15	B1	0	8	WB_oldHARS_29.75	^, 5 degrees alpha
7	50	A4	0	0	8	WB_oldHARS_29.75	negative alpha sweep, more negative data points
8	0	A5	0	0	N/A	WB_oldHARS_29.75	Larger Static Tare
9	0	A6	0	0	N/A	noWB_oldHARS_29.75	Balance and sting only for static balance data
10	50	A7	0	0	N/A	noWB_oldHARS_29.75	PIV on bullet; -16:2:-6
11	50	A8	0	0	N/A	noWB_oldHARS_29.75	PIV on bullet; -6:2:10
12	50	A9	0	0	N/A	noWB_oldHARS_29.75	PIV on bullet; 10:2:16
13	0	A_inv	0	180	N/A	WB_oldHARS_29.75	WB reinstalled, inverted, balance data static
14	50	A_inv	0	180	13	WB_oldHARS_29.75	^, not static
15	50	A8	0	0	N/A	noWB_oldHARS_55.5	long sting, just PIV on bullet
16	0	A6	0	0	N/A	WB_oldHARS_55.5	long sting WB installed, static
17	50	A10	0	0	16	WB_oldHARS_55.5	long sting installed, PIV set up on Bullet
18	50	A10	0	0	16	WB_oldHARS_55.5	
19	50	10	B2	0	16	WB_oldHARS_55.5	Beta sweep, just balance data, 0 degrees alpha
20	50	15	B2	0	16	WB_oldHARS_55.5	^, 5 degrees alpha
21	50	10	0	0	16	WB_newHARS_55.5	PIV only bullet at 10.0deg (8.95)
22	50	A11	0	0	16	WB_newHARS_55.5	8.95 and 14.45 = 10 and 16deg
23	50	A12	0	0	16	WB_newHARS_55.5	10 and 4 degrees on bullet
24	50	A13	0	0	16	WB_newHARS_55.5	
25	50	A13	0	0	16	noWB_newHARS_55.5	
26	0	A5	0	0	N/A	WB_newHARS_55.5	Restarting (just) balance data. Static tare
27	50	A5	0	0	26	WB_newHARS_55.5	alpha sweep
28	50	10	B2	0	26	WB_newHARS_55.5	Beta sweep, 0 degrees alpha
29	50	15	B2	0	26	WB_newHARS_55.5	Beta sweep, 5 degrees alpha
30	0	A5	0	0	N/A	WB_newHARS_29.75	Short Sting installed, Static tare
31	50	A5	0	0	30	WB_newHARS_29.75	alpha sweep
32	50	10	B1	0	30	WB_newHARS_29.75	Beta sweep, 0 degrees alpha
33	50	15	B1	0	30	WB_newHARS_29.75	Beta sweep, 5 degrees alpha
34	0	A_inv	0	180	N/A	WB_newHARS_29.75	Inverted, alpha static
35	50	A_inv	0	180	34	WB_newHARS_29.75	Inverted, alpha sweep
36	0	A5	0	0	N/A	noWB_newHARS_29.75	Short Sting installed, Static tare
37	50	A5	0	0	36	noWB_newHARS_29.75	alpha sweep
38	0	A5	0	0	N/A	WB_newHARS_29.75	Short Sting installed, Static tare
39	50	A5	0	0	38	WB_newHARS_29.75	alpha sweep

OWN - LSWT Test 2014
15-17 September 2020

A0 = 7 tens (zeros), A1 = 0:1:24 (-10:1:14)

12	12	12	10	10	24	30	75
Run Number	Qact (PSF)	Pitch (°)	Yaw (°)	Roll (°)	Static Tare Run Number	Configuration Code	Comments
1	0	A0	0	0	N/A	oldmotors_accels_intbalance	data test, 4sec @ 1024Hz
2	0	A1	0	0	N/A	oldmotors_accels_intbalance	alpha sweep, static, 4sec @ 1024 Hz
3	5	A1	0	0	2	oldmotors_accels_intbalance	alpha sweep, 5q, 4sec @ 1024 Hz
4	10	A1	0	0	2	oldmotors_accels_intbalance	
5	15	A1	0	0	2	oldmotors_accels_intbalance	
6	20	A1	0	0	2	oldmotors_accels_intbalance	
7	0	A0	0	0	N/A	oldmotors_accels_intbalance	mallet whack- nose, 10sec@1024Hz
8	0	A0	0	0	N/A	oldmotors_accels_intbalance	mallet whack- nose, 10sec@1024Hz, motors off
9	0	A0	0	0	N/A	oldmotors_accels_intbalance	mallet whack- tail, 10sec@1024Hz
10	0	A0	0	0	N/A	oldmotors_accels_intbalance	mallet whack- tail, 10sec@1024Hz, motors off

Matt's HARS thesis test part 2 - new motors
OWN - LSWT Test 2018
29-Dec

A0 - 7x10, A1 - 0:1:24 (-10:1:14) (29x10)

12	12	12	10	10	24	30	75
Run Number	Qact (PSF)	Pitch (°)	Yaw (°)	Roll (°)	Static Tare Run Number	Configuration Code	Comments
1	0	A0	0	0	N/A	newmotors_accels_intbalance	data test, 4 sec @ 1024 Hz
2	0	A1	0	0	N/A	newmotors_accels_intbalance	alpha sweep, static tare
3	5	A1	0	0	2	newmotors_accels_intbalance	alpha sweep, 5 q
4	10	A1	0	0	2	newmotors_accels_intbalance	
5	15	A1	0	0	2	newmotors_accels_intbalance	
6	20	A1	0	0	2	newmotors_accels_intbalance	

APPENDIX B

UNCERTAINTY CALCULATIONS

The slope and zero-lift angle of attack results from Figure 4.6 in Chapter 4 were determined using the LINEST function in LibreOffice Calc. This function returns the values and standard errors of the linear fit coefficients.

The $C_L(\alpha)$ plot follows a linear trend given by the following equation:

$$C_L = a(\alpha - \alpha_{L=0}) \qquad (y = mx + b) \tag{B.1}$$

From the results of the linear fit on Figure 4.6 from $\alpha = -8^\circ$ to 5°, the slope m and y-intercept b and their uncertainties σ_m and σ_b are determined by LINEST. The zero-lift angle of attack (x-intercept) and its uncertainty are then determined as follows:

$$\alpha_{L=0} = -b/m \tag{B.2}$$

$$\frac{\sigma_{\alpha_{L=0}}}{\alpha_{L=0}} = \sqrt{\left(\frac{\sigma_b}{b}\right)^2 + \left(\frac{\sigma_m}{m}\right)^2} \tag{B.3}$$

where $m = a = dC_L/d\alpha$ and $b = C_L(\alpha = 0^\circ)$.